https://doi.org/10.5194/essd-2026-564
Preprint. Discussion started: 15 October 2026
© Author(s) 2026. CC BY 4.0 License.



Open Access Earth System Science Data Discussions

Merge Satellite and Gauge Daily Precipitation Data for Areas with Sparse-Gauge and Rugged Terrain: A High-Accuracy Gridded Dataset CGS01 (2000-2024) across China

Bokun Yan[1,3,†], Wenpeng Li[2,*], Fuping Gan[1,3], Yuejun Zheng[2], Juan Bai[1,3], Longfeng Wang[2], Jianrong Li[4], Yi Guo[1,3], Chunyan Li[2], Naichen Xing[1,3], Yue Zhuo[1,3], and Ruoyi Li[1,3]

[1]China Aero Geophysical Survey and Remote Sensing Center for Natural Resources (AGRS), China Geological Survey, Beijing 100083, China
[2]China Institute of Geo-Environmental Monitoring, China Geological Survey, Beijing 100081, China
[3]Key Laboratory of Aero Geophysics and Remote Sensing Geology, Ministry of Natural Resources of the People's Republic of China, Beijing 100083, China
[4]Institute of Hydrogeological and Engineering Geology, Gansu Provincial Bureau of Geology and Mineral Exploration and Development, Zhangye, Gansu 734000, China
*Correspondence: Wenpeng Li, liwenpeng@mail.cgs.gov.cn
†Correspondence: Bokun Yan, yanbokun@mail.cgs.gov.cn

Abstract. High-precision quantification of regional precipitation is the foundation of watershed water balance analysis and water resources management. However, current approaches are hindered by methodological diversity and inconsistent results, with limited accuracy, especially in gauge-sparse regions and areas with drastic topographic relief. This study proposes a dual thin-plate spline (TPS) fusion method combining satellite observations and gauge observations to develop a daily precipitation dataset named CGS01. Multi-dimensional comparisons and comprehensive accuracy evaluations are conducted against several mainstream precipitation products including CN05.1, CMFD_V1 and CHM_PRE_V2. From a methodological perspective, this paper analyzes the core difficulties and feasible solutions for regional precipitation estimation, and discusses the error sources of GPM satellite precipitation data, as well as the application potential of the proposed method in watershed water balance assessment and high-precision global precipitation quantification. The results reveal that compared with digital elevation model (DEM) and reanalysis data used as covariates in TPS method, satellite precipitation data exhibits higher reliability when serving as covariates, while corrections for systematic errors and suppression of random errors are still required. A novel systematic error correction method for GPM data is proposed. Adopting only 27% of the gauge numbers used in previous studies, the newly developed CGS01 presents obviously superior performance to existing datasets. The national average error of annual precipitation is 2.0%. Validated against observed runoff data, the watershed water balance analysis error is 10.9%. Furthermore, CGS01 can reasonably reflect the controlling effects of topography and wind direction on precipitation spatial patterns in high mountain and canyon areas without in-situ observations. Compared with CHM_PRE_V2, CGS01 daily precipitation shows improvements of 14.2%, 2.9%, 21.3%, and 8.2% in the correlation coefficient, Kling-Gupta efficiency, probability of detection, and mean absolute error. The method proposed in this study has three prominent strengths: it requires no preset empirical parameters, delivers highly reproducible results, and imposes low demands on gauge station density. The CGS01 dataset shows that from 2000 to 2024 eight out of China's ten first level watersheds showed annually wetting trends, with

https://doi.org/10.5194/essd-2026-564
Preprint. Discussion started: 15 October 2026
© Author(s) 2026. CC BY 4.0 License.



Open Access Earth System Science Data Discussions

trends ranging from 0.5 to 8.4 mm per year, and in seven of the ten first level watersheds, the contribution ratio of daily extreme precipitation to total precipitation increased at a rate of 0.2%-0.5% per year. Free access to the dataset can be found at https://doi.org/10.5281/zenodo.20176004 (Yan et al., 2026).

1 Introduction

Accurately monitoring precipitation is crucial for water resource management, global climate change adaptation, and the mitigation of flood and drought disasters—hazards that are growing increasingly frequent amid ongoing global warming (Najibi and Devineni, 2018; Yu et al., 2020; Christian et al., 2021; Yu et al., 2022; Wang, 2025). This is because precipitation constitutes a core component of the water and energy cycle of hydrological system (Han et al., 2023; Wang et al., 2024; Hayder and Nassrullah, 2025), and dominates the water availability (Zhang et al., 2023). In numerous water cycle studies such as the urbanization-induced changes in precipitation, water cycle closure, water resource availability, groundwater recharge, and the synergistic changes between air temperature and precipitation, hydrological cycle effects of vegetation change under the background of anthropogenic climate change (Zhang et al., 2023; Miguez-Macho and Fan, 2025; Dorigo et al., 2021; Kuang et al., 2024; Cohen and Pincus, 2025; Gebrechorkos et al., 2025; Zhang et al., 2022), the uncertainty of precipitation data and the inconsistency of data sources are non-negligible causes of research uncertainty, especially in gauge-sparse areas (Zhang et al., 2024; Su et al., 2026).

It is a great challenge to accurately monitor precipitation distribution solely using gauge observations and ground-based radar technology, owing to the remarkable spatiotemporal variability of precipitation. This challenge is particularly pronounced in gauge-sparse watersheds, such as the Tibetan Plateau in China—a region known as the “Third Pole” and a global hotspot for hydrological research—where the extremely low gauge density is a major bottleneck hindering the understanding of hydrological cycle processes (Yang et al., 2023). For instance, the Qiangtang Basin on the Tibetan Plateau covers an area of 220,000 km^2 but is equipped with only four meteorological gauges in the China National Meteorological Network. Similarly, in the Xinjiang Uygur Autonomous Region, gauges are predominantly deployed in plain areas, whereas most precipitation events occur in mountainous regions (Wang et al., 2020; Jin et al., 2024).

Thus, interpolating unevenly and sparsely distributed gauge precipitation data to generate gridded precipitation products is critical for hydrological and meteorological research (Wei et al., 2023). A variety of interpolation methods have been developed for this purpose, with many incorporating digital elevation model (DEM) or reanalysis data to correct the effects of topography and distance from the coastline on precipitation, such as CN05.1, CMA_V2.0, CHM_PRE_V1, and CMFD_V1 (Wu and Gao, 2013; He et al., 2020; Han et al., 2023; Zhang et al., 2024). Thin Plate Spline (TPS) interpolation, being adept at fitting the spatially smooth variations of precipitation fields, performs well compared to other methods and does not require the manual setting of empirical parameters and can incorporate DEM as a covariate to quantify the topographic effects on precipitation (Hutchinson, 1995; Hutchinson et al., 2009; Zhang et al., 2024). The statistical regression model referred to as PRISM (Parameter-Elevation Regressions on Independent Slopes Model) has been adopted in the production of CHM_PRE_V1 to describe the topographic effects on the monthly precipitation field (Han et al., 2023).

https://doi.org/10.5194/essd-2026-564
Preprint. Discussion started: 15 October 2026
© Author(s) 2026. CC BY 4.0 License.



Satellite-based precipitation products (SPPs), which can provide global coverage with fine spatiotemporal resolution, are of great value—particularly for gauge-sparse and topographically rugged regions—and have been extensively applied in climatic and hydrological research (Liu et al., 2022; Pan et al., 2023). Commonly used SPPs include CMORPH, TRMM, GPM-GSMaP, and GPM-IMERG (Huffman et al., 2007; Joyce et al., 2004; Mega et al., 2019; Shen and Xiong, 2022). Among these, GPM-GSMaP and GPM-IMERG are the successor and upgraded versions of TRMM; these two products integrate radar, microwave, and infrared data, and are recognized as the most widely used and reliable SPPs to date (Liu et al., 2020, 2022; Pan et al., 2023).

Despite their considerable application potential, SPPs exhibit substantial uncertainties and biases stemming from topography, precipitation intensity, observation frequency, and precipitation retrieval algorithms (Fang et al., 2019; Tang et al., 2022). Therefore, it is necessary to merge gauge observations with SPPs to reduce such errors. This is especially critical for gauge-sparse and topographically rugged areas, where the accuracy of both satellite-derived and gauge-based precipitation data remains to be improved (Zhang and Wang, 2023).

Numerous methods have been proposed for merging SPPs and gauge precipitation data. Optimal interpolation (OI) corrects the systematic bias of SPPs under the assumption that the bias is multiplicative, and reduces random errors by merging SPPs with gauge data (Nie et al., 2016). The performance of this method is largely dependent on gauge density, which exerts a significant impact on the bias correction (i.e., systematic error correction) of SPPs—a procedure conducted prior to OI implementation (Nie et al., 2016). Besides, the calculation of the weight matrix in OI is subjective and cumbersome (Nie et al., 2016).

Linearized weighting (LW) and inverse root-mean-square error weighting (IRMSE) (Woldemeskel et al., 2013; Yang et al., 2017), merge SPPs and gridded gauge data by summing the two weighted components, such that the data with lower error variance or root-mean-square error (RMSE) is assigned a larger weight in the merged result. It is worth noting that error variance only reflects random errors, while RMSE incorporates both systematic and random errors, leading to inherent differences in their weighting effects.

The bias correction method based on multiple linear regression (BMLR) establishes a linear relationship between SPP biases and influencing factors (e.g., longitude, latitude, slope, and topographic aspect) to correct the biases of SPPs (Daly et al., 2002; Tang et al., 2022). As one of the most prevalent machine learning methods, random forest (RF) outperforms linear regression in capturing the nonlinear variability of precipitation and has been applied to precipitation prediction by integrating SPPs with covariates (Baez-Villanueva et al., 2020; Zhang et al., 2021). Apart from RF, other methods such as light gradient boosting machine (LGBM) algorithm has been used to in the production of CHM_PRE_V2 (Hu et al., 2025). However, this kind of nonlinear methods, including deep learning-based methods (Hu et al., 2025; Jiang et al., 2025), have the problem that errors are highly prone to amplification during interpolation and extrapolation (Daly et al., 2002).

Despite the availability of diverse interpolation methods and gridded datasets—derived from gauge observations, satellite remote sensing, and reanalysis data—precipitation quantification accuracy remains inadequate. Notably, even with the same input data, different interpolation methods often yield inconsistent results (Han et al., 2023). These issues, coupled with insufficient data accuracy, have greatly constrained research on global climate change and watershed water balance analysis. Currently, the hydrological community generally adopts two methods to mitigate the impact of inaccurate quantification of precipitation

https://doi.org/10.5194/essd-2026-564
Preprint. Discussion started: 15 October 2026
© Author(s) 2026. CC BY 4.0 License.



data: one is to use the method of averaging multiple datasets (Zhang et al., 2023), and the other is to select the best datasets according to the accuracy evaluation based on in-situ gauge observations (Zhang et al., 2024). The first method may reduce errors, but it may also increase the overall error by introducing data sources with large errors; the second method is more suitable for regions with dense gauge stations. Currently, the accuracy evaluation of different methods and products mostly focuses on the spatial dimension. In addition to regional distribution, the temporal variation patterns of precipitation are also an important part of hydrological cycle research. To ensure data reliability, it is necessary to evaluate data accuracy from both spatial and temporal dimensions.

To address the issues of diverse regional precipitation quantification methods, insufficient accuracy, and the resultant hindrance to deepening the understanding of global and basin-scale hydrological cycle patterns, it is necessary to start with the analysis of method principles and applicability, quantify systematic and random errors, and design an optimal scheme for regional precipitation quantification in accordance with the basic principle of "correcting systematic errors based on the error characteristics and suppressing random errors through weighted averaging of multi-source data" to improve data consistency in hydrological research. This study quantifies the errors of GPM and gauge interpolation, proposes a set of GPM-gauge precipitation merging schemes, and conducts a more comprehensive evaluation of the accuracy of this scheme and other representative datasets from both spatial and temporal dimensions.

2 Materials and methods

2.1 Study area

The western part of the study area is characterized by sparse gauges and significant topographic relief, with an altitude difference exceeding 8,000 meters—factors that render it a challenging area for regional precipitation quantification. Furthermore, as a semi-arid and arid zone with scarce water resources, the western region is also a key focus for regional precipitation quantification and water resource assessment (Figure 1).

2.2 Data

The data includes daily precipitation data from gauges, Global Precipitation Measurement (GPM) data, and other gridded precipitation datasets employed for comparison and cross-validation include CN05.1 (2000-2023) (Wu and Gao, 2013), CMFD_V1 (2000-2018) (He et al., 2020), and CHM_PRE_V2 (2000-2024) (Zhang et al., 2024).

A total of 2125 gauges are used in this study. Of these, 2053 gauges are located in mainland China and obtained from the China Meteorological Administration (CMA; https://data.cma.cn). The remaining 72 gauges are acquired from the Global Historical Climatology Network-Daily (GHCN-D), maintained by the National Centers for Environmental Information (NCEI, formerly NCDC) of the National Oceanic and Atmospheric Administration (NOAA; https://www.ncei.noaa.gov). Of the 2053 Chinese gauges, 657 have continuous observations for 2000–2024 and are used for data merging. An additional 1468 gauges cover 2022–2024 and are used exclusively for accuracy assessment. Satellite precipitation data are obtained from the GPM IMERG

https://doi.org/10.5194/essd-2026-564
Preprint. Discussion started: 15 October 2026
© Author(s) 2026. CC BY 4.0 License.



Open Access Earth System Science Data Discussions

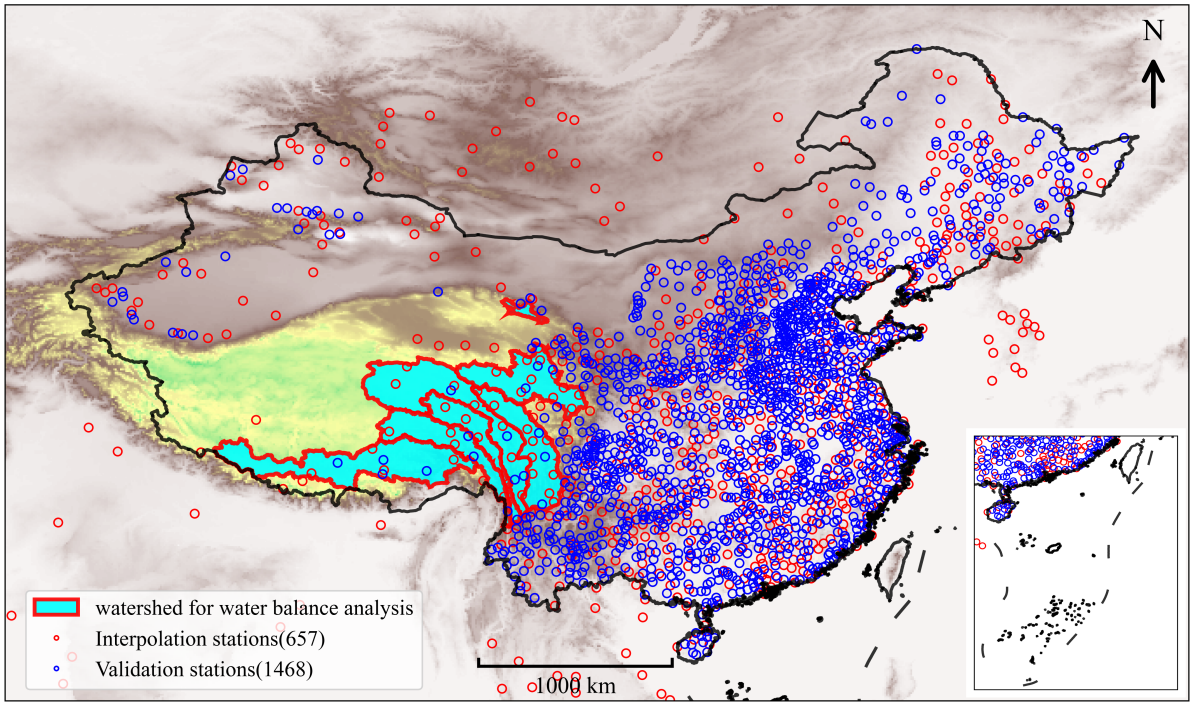


Figure 1. Meteorological stations distribution.

Version 07 Final Run product, provided by the National Aeronautics and Space Administration (NASA; https://www.nasa.gov). The runoff data (2005–2022) adopted for water balance analysis and the water resources volume data of national first-level basins were collected from the Water Resources Bulletin issued by the Ministry of Water Resources of the People's Republic of China (http://www.mwr.gov.cn/).

2.3 Methods

The overall technical procedure is as follows: annual precipitation data are first generated, and then daily precipitation is produced according to the proportion of daily precipitation in the annual total precipitation (Figure 2). For annual precipitation, systematic error correction is first performed on GPM annual precipitation data. Then, the two-dimensional thin-plate spline method is adopted to fuse it with gauged annual precipitation data. The resulting annual precipitation product not only retains the advantage of fine spatial distribution of GPM data, but also features high local accuracy of gauge observations. For daily precipitation, a weighted fusion method is used to integrate gridded daily precipitation data interpolated by the two-dimensional thin-plate spline method with GPM daily precipitation. Weights are determined by the random error of each dataset, with a higher weight assigned to the data with smaller errors. The fused daily precipitation is divided by the corresponding annual precipitation to obtain the daily precipitation proportion factor, which characterizes the contribution of each daily precipitation to the annual total.

https://doi.org/10.5194/essd-2026-564
Preprint. Discussion started: 15 October 2026
© Author(s) 2026. CC BY 4.0 License.

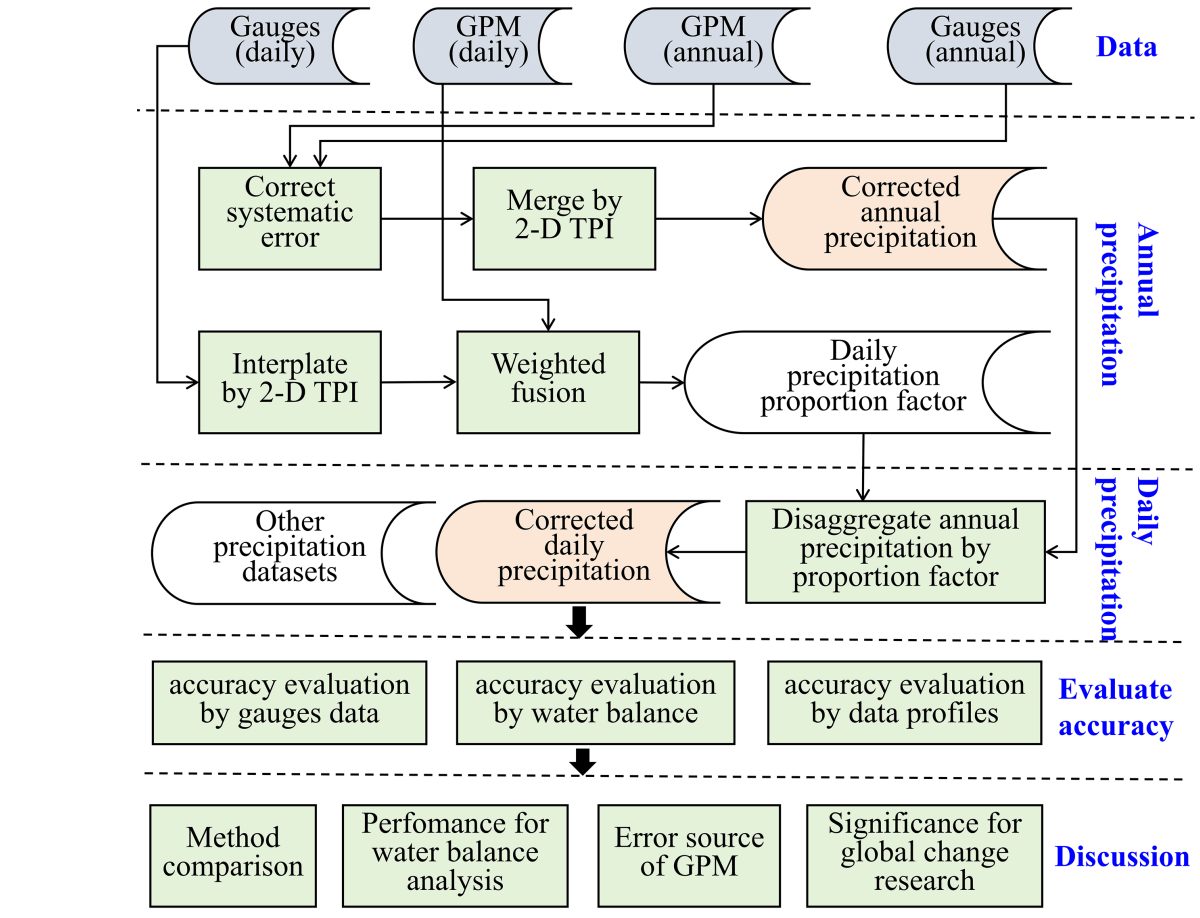


Figure 2. Flowchart for data merge.

Both annual and daily precipitation generation employ the two-dimensional thin-plate spline method. Although the core algorithm is consistent, the specific settings differ: for annual precipitation, the systematically error-corrected GPM data are used as covariates, and the degree of smoothness is automatically solved via generalized cross-validation; for daily precipitation, no covariates are introduced, and the degree of smoothness is set to 0 (Hutchinson, 1995).

Three types of approaches are adopted in this study for accuracy assessment: first, quantitative validation based on independent gauge stations; second, watershed water balance analysis, in which watersheds with weak human activities and relatively stable hydro-physical underlying surfaces are selected, and runoff is simulated using the Budyko model (Ma et al., 2024) and compared with observed runoff; third, data profile analysis, in which the coupling relationship between the spatial distribution of precipitation and topography as well as wind direction is examined in regions with large topographic relief and sparse gauges. The above multi-dimensional accuracy verification can comprehensively ensure the accuracy and reliability of the dataset.

https://doi.org/10.5194/essd-2026-564
Preprint. Discussion started: 15 October 2026
© Author(s) 2026. CC BY 4.0 License.



Finally, discussions are conducted on issues of widespread concern in the research community: first, method comparison and analysis, aiming to identify a reasonable technical route in response to the diversity and inconsistency of existing regional precipitation generation methods; second, performance evaluation of the dataset in watershed water balance analysis, providing a reference for solving the long-standing water balance closure problem in hydrology (Dorigo et al., 2021); third, analysis of error sources in GPM satellite precipitation data; fourth, discussion on the application value and scientific significance of the proposed method in global change research.

2.3.1 Quantify systematic and random error

In this study, a two-step scheme is adopted: first generating fused annual precipitation grids, and then producing grids of the intra-annual proportion of daily precipitation. In the construction of annual precipitation grids, GPM annual precipitation is used as an interpolation covariate to characterize the high-frequency spatial variability of precipitation induced by topographic factors (elevation, slope, aspect) and wind direction. However, the systematic error of GPM annual precipitation must first be quantified and corrected. In the generation of grids for the intra-annual proportion of daily precipitation, weighted fusion is performed based on the random errors of GPM and gauge-interpolated results to suppress random errors. Therefore, it is necessary to quantify the random errors of GPM and interpolated daily precipitation data separately.

For annual precipitation, in the two-dimensional scatter plot consisting of gauges (x) and GPM (y) data, the x-values are divided into several intervals with an equal number of samples in each interval. The mean and standard deviation of x and y within each interval are then calculated. The difference between the mean y and mean x in each interval is taken as the systematic error of GPM for the corresponding precipitation interval, and one standard deviation of y is taken as its random error (Figure 3 and Figure 4). For GPM daily precipitation, the same interval division method is applied, and one standard deviation of y in each interval is used as the random error of GPM for different precipitation intervals.

2.3.2 Correct the systematic error of GPM

Using a daily mean air temperature of 273.15 K as the threshold, GPM daily precipitation is classified into snowfall and rainfall ($\geq$ threshold as rainfall, $<$ threshold as snowfall) (Maina and Kumar, 2025). The systematic and random errors of annual snowfall and annual rainfall are then quantified separately. Results show that the systematic error of snowfall exhibits strong linear consistency with annual snowfall amount: the systematic error becomes increasingly negative with increasing annual snowfall, and satisfactory correction can be achieved using linear calibration. Notably, the linear correction formula should not be directly fitted from raw snowfall data, but derived from the mean values obtained by segmental calculation (Figure 3). The systematic error of annual rainfall shows a nonlinear relationship with annual rainfall amount, presenting an overall S-shaped distribution: the systematic error is negative in high rainfall ranges, positive in medium–low rainfall ranges, and smaller in low rainfall ranges than in medium rainfall ranges. Therefore, a piecewise linear correction method is adopted, assuming that the systematic error varies linearly within a narrow rainfall interval (Figure 4).

Although the data in the annual precipitation comparison scatter plot do not deviate significantly from the 1:1 line, the influence of the S-shaped systematic error cannot be ignored and must be corrected for the following reasons:(1) Although the distribution

https://doi.org/10.5194/essd-2026-564
Preprint. Discussion started: 15 October 2026
© Author(s) 2026. CC BY 4.0 License.

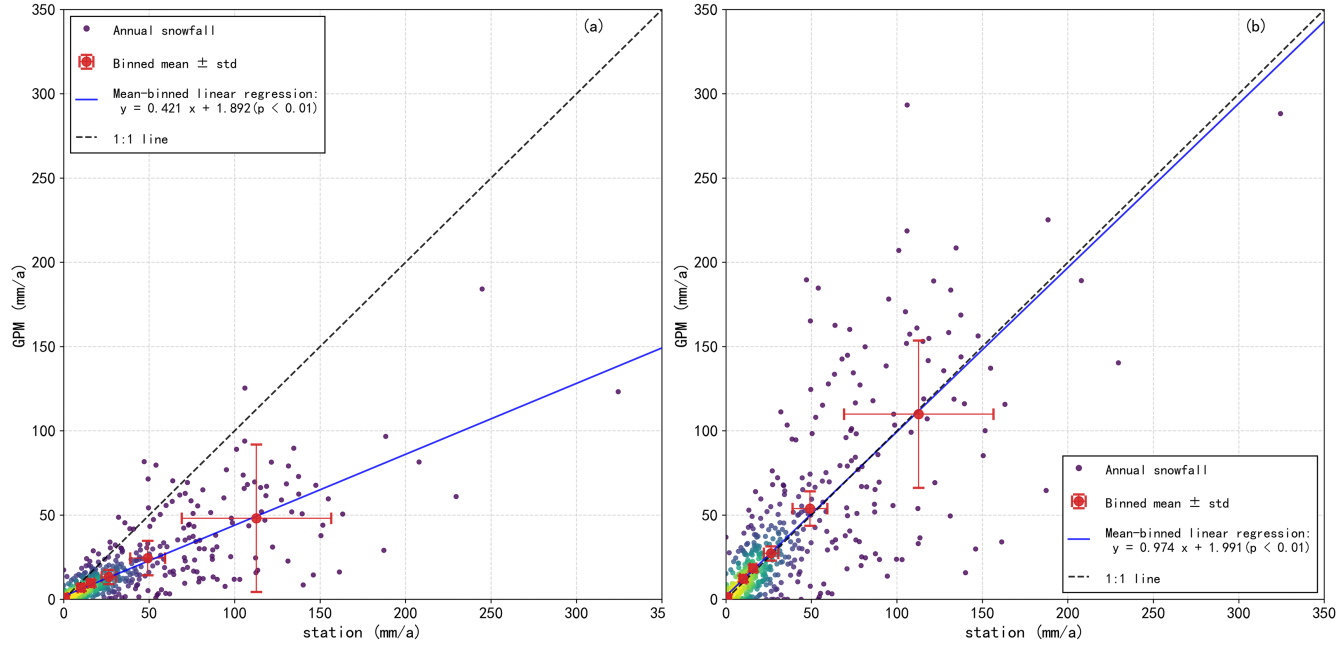


Figure 3. Annual snowfall corrected via the mean-binned linear regression method. It should be noted that the systematic bias cannot be rectified by direct linear regression of raw annual snowfall data, but only by the linear regression of binned mean values. (a) GPM-derived annual snowfall exhibits an underestimation relative to station observations, with the systematic bias showing a strong linear correlation with station-measured annual snowfall. (b) The systematic bias is effectively corrected using the mean-binned linear regression method.

pattern of systematic error is generally similar across years, certain differences exist. Without correction, this will lead to unpredictable distortions in long-term precipitation trends, and inter-annual precipitation variability is a key parameter in hydrological analysis. (2) In the medium–low rainfall range, small systematic errors can induce considerable relative errors. Watershed water balance analysis is highly sensitive to relative errors, especially in arid and semi-arid regions.

2.3.3 Merge daily precipitation of GPM and gauges interpolation

The two datasets are merged using the weighted summation method. The merging weights are determined based on the error variances of the two datasets, following the linear weighting scheme proposed by Woldemeskel et al. (Woldemeskel et al., 2013): a higher weight is assigned to the dataset with a smaller error variance, ensuring that the merged result is dominated by the more accurate data source. Based on 1468 validation gauges, the error variances of GPM daily precipitation and daily precipitation interpolated by the two-dimensional thin-plate spline method are calculated separately, and their respective merging weights are then derived according to Equations (1) and (2).

As these validation gauges only have observations from 2022 to 2024, the random errors for other years are represented by the average values over 2022–2024. During 2022–2024, the weight of GPM data ranges from 0.51 to 0.58 with a mean of 0.54,

https://doi.org/10.5194/essd-2026-564
Preprint. Discussion started: 15 October 2026
© Author(s) 2026. CC BY 4.0 License.

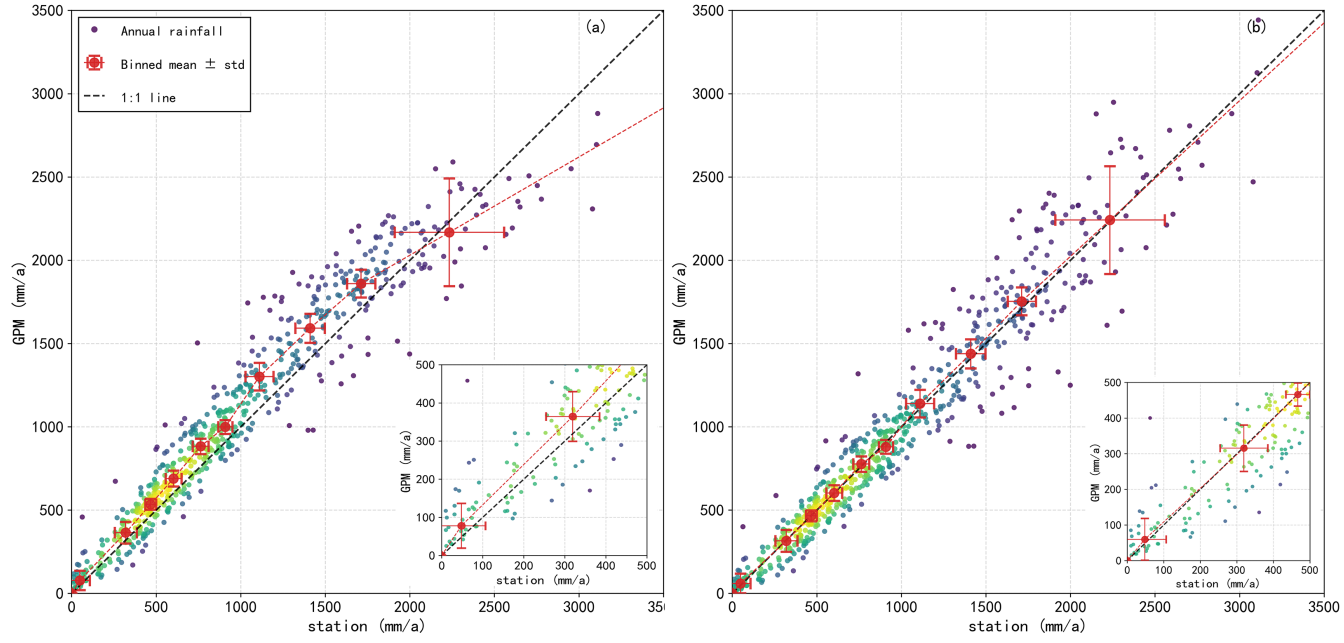


Figure 4. Annual rainfall corrected by the mean-binned piecewise linear regression method. (a) GPM-derived annual rainfall exhibits an overestimation at low-mid rainfall and underestimation at high rainfall relative to station observations, i.e. "S-shaped" nonlinear systematic bias. (b) The "S-shaped" nonlinear systematic bias is effectively corrected using the piecewise mean-binned linear method.

while the weight of the interpolated data ranges from 0.42 to 0.49 with a mean of 0.46. Given the small inter-annual variation in weights, it is reasonable to apply the 2022–2024 average weights for the period 2000–2021. Weights are determined according to the random variance of each precipitation dataset:

$$w_1 = \frac{\sigma_2^2}{\sigma_1^2 + \sigma_2^2} \tag{1}$$

$$w_2 = \frac{\sigma_1^2}{\sigma_1^2 + \sigma_2^2} \tag{2}$$

where σ_1 and σ_2 denote the variance of GPM precipitation and gauge observation, respectively; w_1 and w_2 are the fusion weights corresponding to GPM and gauge station data.

2.3.4 Accuracy evaluation

The accuracy evaluation metrics using validation stations as the "ground truth" include: Correlation Coefficient (CC), Kling-Gupta Efficiency (KGE), Probability of Detection (POD), False Alarm Ratio (FAR), Relative Bias (BIAS), and Mean Absolute Error (MAE). The calculation formulas are referenced from Hu et al. (Hu et al., 2025) and Yu et al. (Yu et al., 2022).

https://doi.org/10.5194/essd-2026-564
Preprint. Discussion started: 15 October 2026
© Author(s) 2026. CC BY 4.0 License.



3 Results

3.1 Distribution of annual precipitation and its relationship with orography

Although the overall spatial distribution patterns of precipitation are relatively consistent across the products, non-negligible differences exist among them (Figure 5). CGS01 and CMFD_V1 show a more pronounced influence of topography on precipitation in western China. Although topographic effects can also be observed in CN05.1, its spatial details are less distinct. CHM_PRE_V2 performs poorly in capturing the topographic influence on precipitation. The maximum precipitation values also vary to some extent. The highest value in CGS01 is located in the southeastern Qinghai-Tibet Plateau, reaching over 4,700 mm/a. CMFD_V1 and CHM_PRE_V2 also identify this region as a high-precipitation zone, but with much lower magnitudes, and CN05.1 yields even lower values.

Seven transects were selected across the Qinghai-Tibet Plateau and Tianshan Mountains to analyze the spatial variation in precipitation and its relationships with topography and wind direction. Results show that the patterns revealed by CGS01 are significantly more consistent with topography and wind direction than those of the other three datasets, mainly in the following aspects: First, precipitation usually peaks on the monsoon windward slopes near the summits of high mountains. Second, precipitation in the upwind monsoon regions is generally higher than that in the downwind regions. Third, local variations in precipitation are strongly controlled by topography, with precipitation at high altitudes generally greater than that at low altitudes. CHM_PRE_V2, CMFD_V1, and CN05.1 fail to adequately capture the above regularities (Figure 6).

In the western Qinghai-Tibet Plateau, along the south-to-north transect (A–B–C), precipitation increases rapidly from the plain toward the Himalayas, peaks near the main ridge, then decreases sharply, reaching a minimum south of the Kunlun Mountains in the northern Qinghai-Tibet Plateau. This region is dominated by the Indian monsoon. Along the north-to-south transect (C–B), precipitation peaks on the northern slope of the Kunlun Mountains and drops rapidly to a minimum after crossing the range. Along the south-to-north transect (E–D) across the Tanggula Mountains, precipitation generally decreases, controlled mainly by the southeast monsoon, and varies synchronously with topographic fluctuations. In the southeastern Qinghai-Tibet Plateau, along the transect from south to northeast (F–G), precipitation reaches its maximum on the southern windward slope of the mountains and then decreases sharply, dominated by the Indian monsoon and modulated by topography. For the Tianshan transects (J–K, L–M), water vapor is mainly supplied by the westerlies from the northwest. Due to its inland location and limited moisture availability, precipitation is concentrated on the northern windward slope, and declines to a minimum over a shorter distance after crossing the mountains. The CGS01 dataset can reasonably explain the effects of wind direction, elevation, and topographic drag on spatial precipitation variability (Jiang et al., 2022).

3.2 Annual Runoff Simulation and Accuracy Validation Based on the Budyko Model

Gauge stations have limited spatial representativeness, especially when station density is low, making it difficult to effectively evaluate the accuracy of data in the temporal dimension. Therefore, at the watershed scale, this study simulates runoff based on the Budyko model and compares it with observed runoff for accuracy assessment. If the two are in good agreement, it indicates

https://doi.org/10.5194/essd-2026-564
Preprint. Discussion started: 15 October 2026
© Author(s) 2026. CC BY 4.0 License.

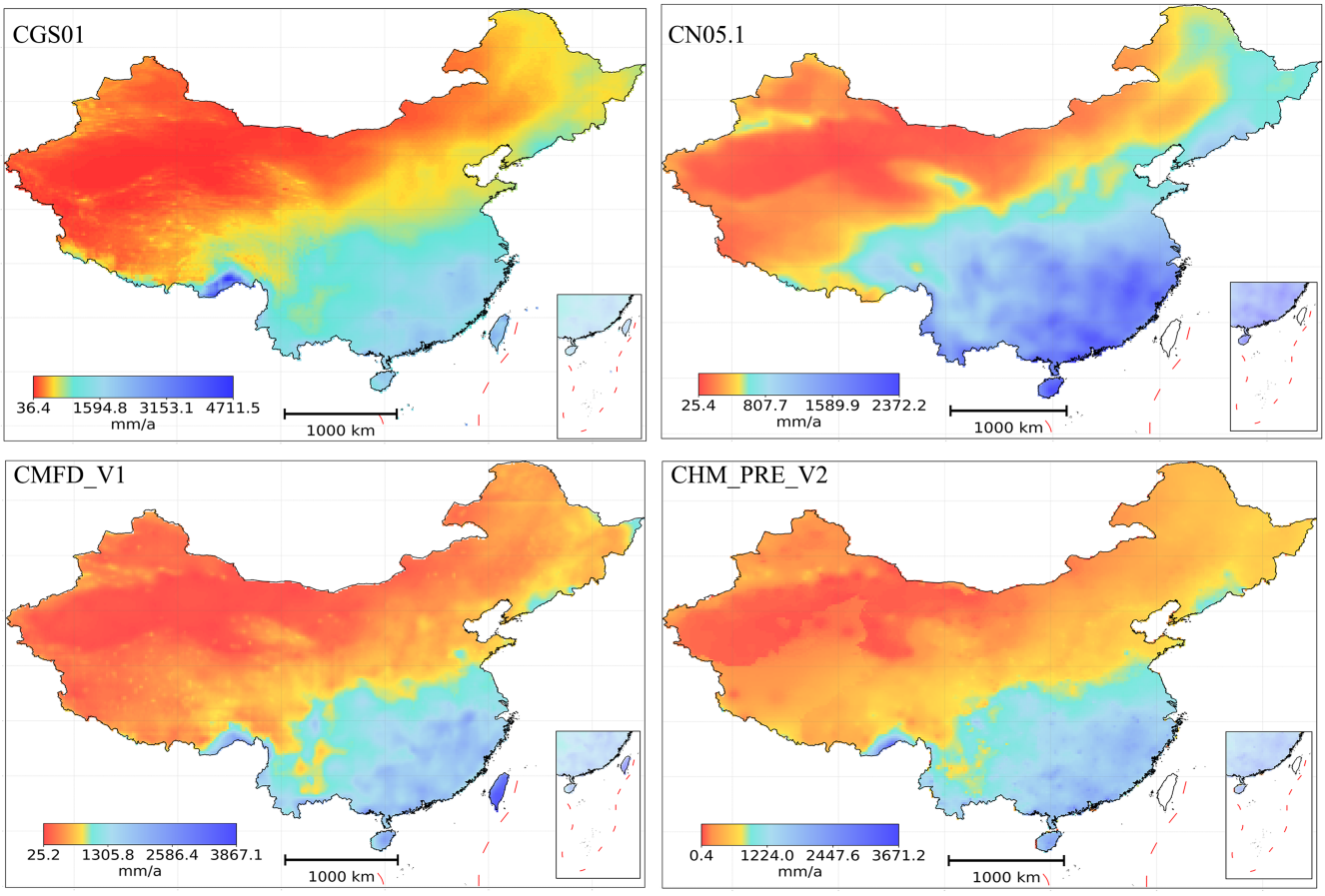


Figure 5. Distribution of average annual precipitation (2000-2018). Although the overall spatial distribution characteristics of precipitation are relatively consistent among different products, non-negligible differences still exist between them. CN05.1 fails to capture the precipitation extreme center in the southeastern Qinghai-Tibet Plateau and does not finely depict the topographic control on precipitation distribution. CMFD_V1 shows that precipitation in Taiwan Province is higher than that in the extreme precipitation region of the southeastern Qinghai-Tibet Plateau. CHM_PRE_V2 cannot adequately reflect the control of topography on the spatial distribution of precipitation.

that precipitation and runoff from independent data sources are highly consistent and conform to the laws of the water cycle, suggesting that the precipitation data have high reliability in the temporal dimension.

CHM_PRE_V2, CGS01, and CMFD_V1 exhibit very similar performance in terms of both relative root mean square error and trend bias, and are significantly superior to CN05.1. Among the three, CHM_PRE_V2 performs the best, while CGS01 is very close to it (Figure 7 and Figure 8). Specifically, the relative root mean square error is defined as the root mean square error of simulated annual runoff divided by the multi-year mean observed annual runoff. The trend bias is defined as the difference between the multi-year mean trend of simulated annual runoff and that of observed annual runoff, divided by the multi-year mean observed annual runoff. The multi-year mean trend is calculated using the Theil-Sen median slope method. This method

https://doi.org/10.5194/essd-2026-564
Preprint. Discussion started: 15 October 2026
© Author(s) 2026. CC BY 4.0 License.

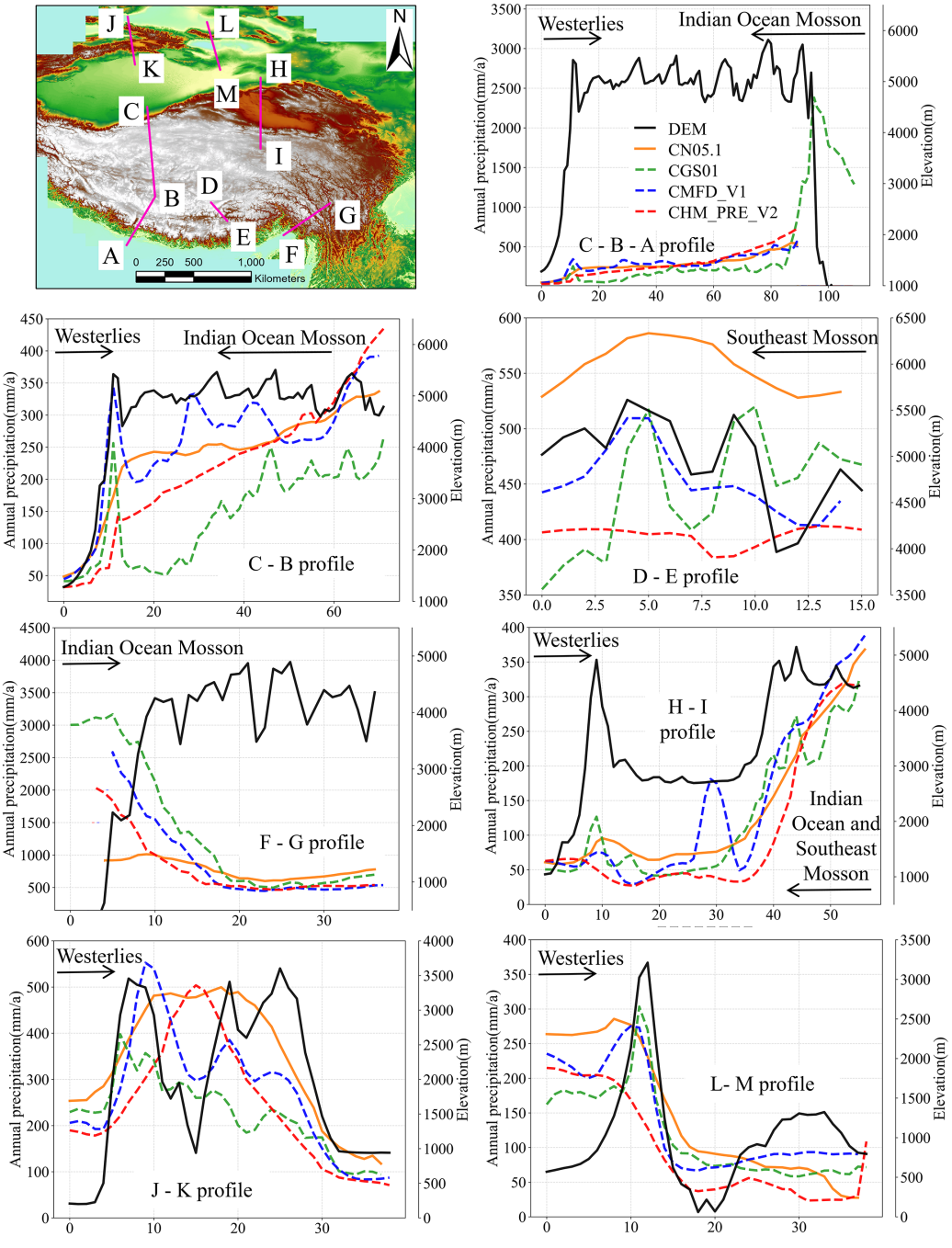


Figure 6. Comparison of elevation (DEM) and average annual precipitation profiles. The spatial variation of precipitation is jointly controlled by wind direction and topography. The CGS01 dataset can reasonably explain the effects of wind direction, elevation, and topographic drag on spatial precipitation variability (Jiang et al., 2022).

https://doi.org/10.5194/essd-2026-564
Preprint. Discussion started: 15 October 2026
© Author(s) 2026. CC BY 4.0 License.



computes slopes between all pairs of data points and takes the median rather than the mean, thereby resisting the influence of extremely high or low annual runoff values and yielding a more stable slope that better reflects the overall changing trend.

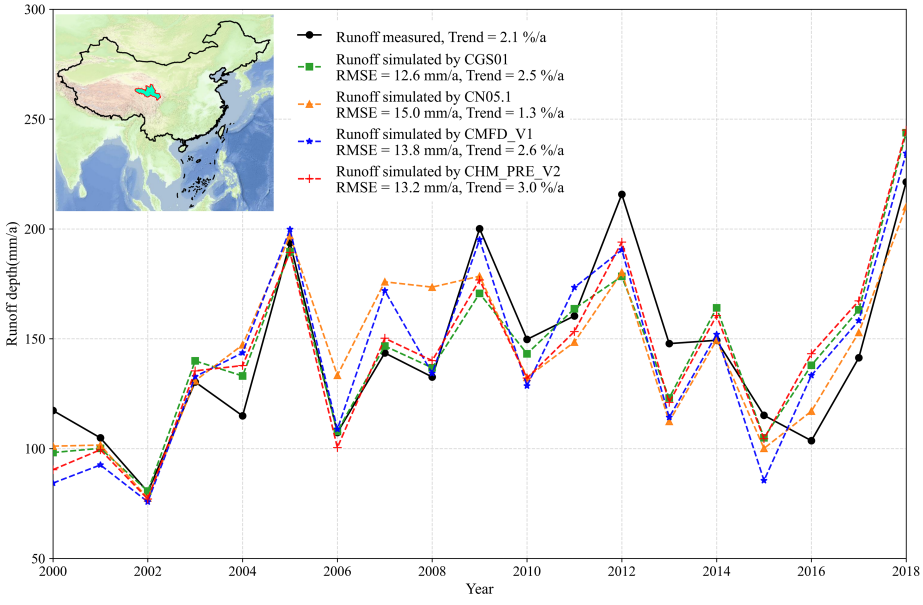


Figure 7. Comparison Between Runoff Simulated by Different Precipitation Products and Measured Runoff in the Upper Reaches of the Yellow River Basin.

3.3 Accuracy Evaluation Based on Validation Gauges

Validation stations can reflect the reliability of precipitation products in spatial distribution to a certain extent. Based on these validation gauges, the accuracies of CGS01, GPM, CHM_PRE_V2, and CN05.1 were evaluated across different annual precipitation intervals(Figure 9). GPM shows overestimation over all intervals, which is another manifestation of its S-shaped systematic error pattern(Figure 4). CGS01 significantly corrects this overestimation in all precipitation ranges and greatly reduces the error, but still exhibits obvious overestimation in the weak precipitation interval (0–200 mm). This indicates that the scarcity of gauges used for calculating systematic error in the weak precipitation range affects the statistical accuracy of systematic error correction. CHM_PRE_V2 has very small errors across all precipitation bins, nearly zero, suggesting high consistency between its gridded precipitation and gauge observations at validation sites. However, considering that these validation gauges were already used as modeling gauges in the interpolation of CHM_PRE_V2 and are not independent samples, it is inappropriate to conclude that this product has the highest accuracy based solely on such results. CMFD_V1 lacks data covering 2022–2024, whereas the gauge validation period adopted in this study spans 2022 to 2024. Consequently, the annual precipitation errors of CMFD_V1 cannot be quantified.

https://doi.org/10.5194/essd-2026-564
Preprint. Discussion started: 15 October 2026
© Author(s) 2026. CC BY 4.0 License.



Open Access Earth System Science Data Discussions

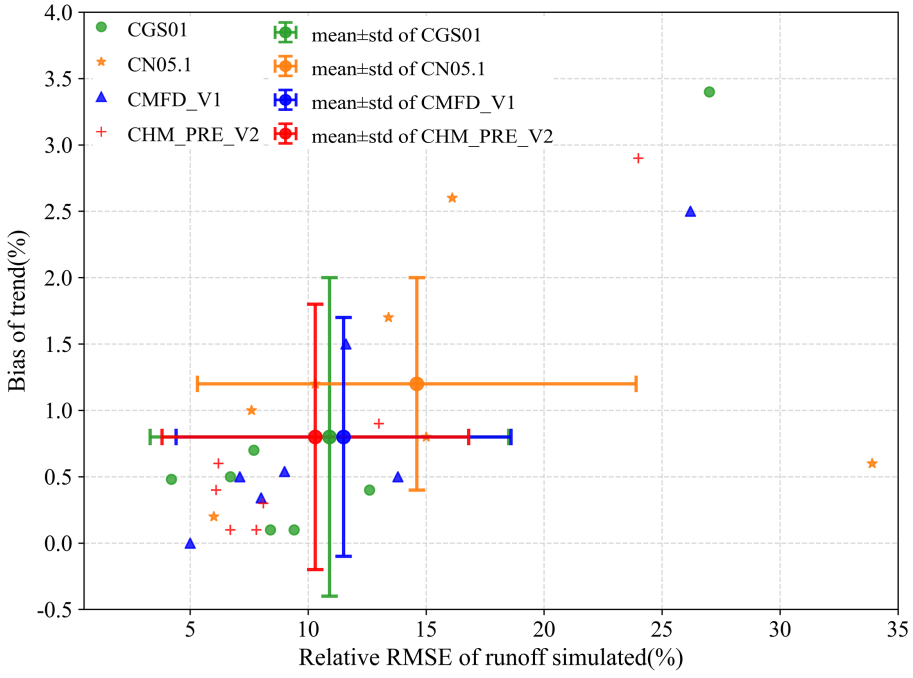


Figure 8. Error of water balance analysis by Budyko model. Relative RMSE is ratio of RMSE and measured runoff.

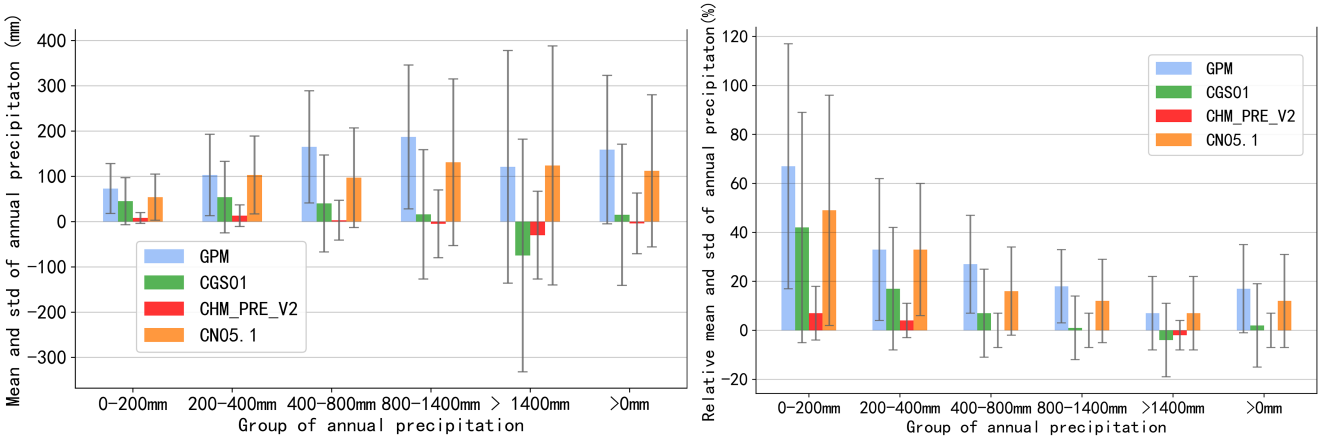


Figure 9. Error of annual precipitation. (a)Mean and standard deviation of annual precipitation (2022-2023); (b)Relative mean and standard deviation of annual precipitation (2022-2023).

https://doi.org/10.5194/essd-2026-564
Preprint. Discussion started: 15 October 2026
© Author(s) 2026. CC BY 4.0 License.



Open Access Earth System Science Data Discussions

For precipitation intervals of 0–200 mm, 200–400 mm, 400–800 mm, 800–1400 mm, >1400 mm, and >0 mm, the mean relative errors are 42%, 17%, 7%, 1%, -4%, and 2% for CGS01; 7%, 4%, 0%, 0%, -2%, and 0% for CHM_PRE_V2; 49%, 33%, 16%, 12%, 7%, and 12% for CN05.1; and 67%, 33%, 27%, 18%, 7%, and 17% for GPM, respectively (Figure 9). The mean relative error is defined as the mean of errors divided by the mean precipitation at gauge sites, which is identical to the relative bias.

The accuracy of daily precipitation from CGS01, GPM, and CHM_PRE_V2 was evaluated against gauge observations. Daily precipitation data for CN05.1 were not available, so its accuracy assessment was not conducted. Given that CN05.1 performed the worst in the above annual precipitation evaluation, it is unnecessary to further evaluate its daily accuracy. CGS01 outperforms GPM and CHM_PRE_V2 significantly in terms of correlation coefficient (CC), Kling-Gupta efficiency (KGE), probability of detection (POD), and mean absolute error (MAE). CGS01 has a similar false alarm ratio (FAR) to GPM but a greatly improved relative bias (RB), while CHM_PRE_V2 performs notably better in these two metrics (Figure 10). The remarkably low FAR of CHM_PRE_V2 is mainly attributed to its two-step machine learning framework:it first classifies precipitation and non-precipitation pixels, and then models precipitation amounts only for precipitating pixels. Its small RB indicates that errors are less likely to accumulate when annual precipitation is accumulated from daily values, which is also verified by the high consistency between its annual precipitation and gauge observations (Figure 7). Based on the daily precipitation scatter plots between CGS01 and CHM_PRE_V2 and the above accuracy metrics(Figure 11), we conclude that at the daily scale, although CHM_PRE_V2 exhibits smaller FAR and RB, its correlation and consistency with gauge observations are weaker than those of CGS01. Moreover, the validation stations are independent of CGS01 (not used in model training) but non-independent for CHM_PRE_V2. Therefore, the reliability of CGS01 daily precipitation is superior to that of CHM_PRE_V2.

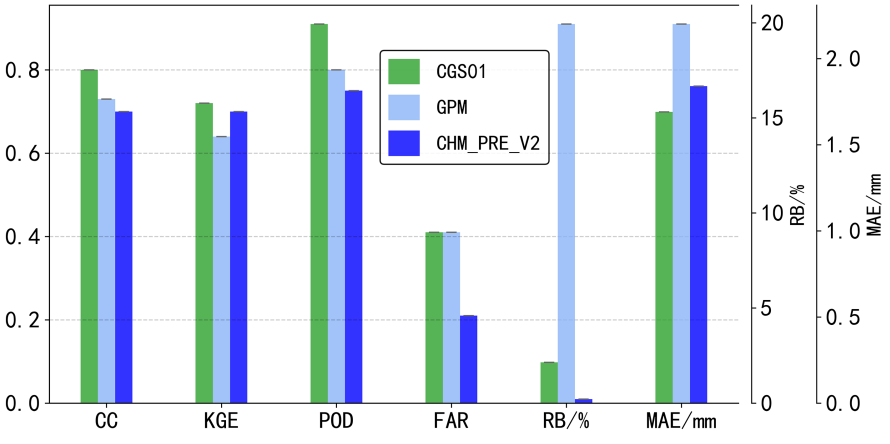


Figure 10. Statistics of accuracy of daily precipitation(2022-2023).

The correlation coefficient, KGE, POD, and MAE of CGS01 are 0.80, 0.72, 0.91, and 1.69 mm/d, respectively, while those of CHM_PRE_V2 are 0.70, 0.70, 0.75, and 1.84 mm/d. Compared with CHM_PRE_V2, CGS01 shows improvements of 14.2%,

https://doi.org/10.5194/essd-2026-564
Preprint. Discussion started: 15 October 2026
© Author(s) 2026. CC BY 4.0 License.

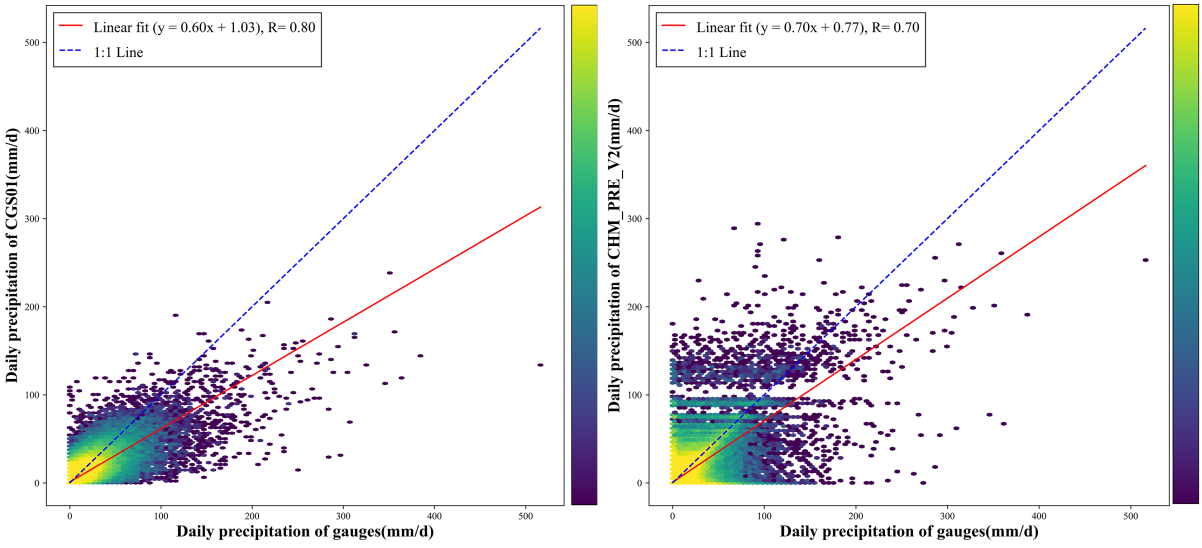


Figure 11. Scatter chart of CGS01 and CHM_PRE_V2(2022-2023).

2.9%, 21.3%, and 8.2% in the above indicators, respectively (Figure 10). The daily precipitation accuracy of CHM_PRE_V2 calculated in this study differs from the results reported by its original authors(Hu et al., 2025). The discrepancy is presumably due to differences in the gauge datasets used. Since identical station data were employed for both CGS01 and CHM_PRE_V2 in this study, it can be confirmed that the former outperforms the latter in terms of accuracy.

3.4 Precipitation and Its Trends in China and First-Level Watersheds

There are certain discrepancies in annual precipitation and its trend rate among various precipitation products across China and its first-level river basins. Combined with the error analysis above, the results from CGS01 show the highest reliability. The trend rate is calculated using the Theil-Sen median slope method, which computes slopes between all pairs of data points and takes the median rather than the mean to reduce the influence of extremely high or low annual precipitation values, yielding a more stable and representative overall trend. The trend rate is estimated at the 95% confidence level.

CN05.1 exhibits obviously higher precipitation than CGS01, CHM_PRE_V2, and CMFD_V1 across China and most first-level basins except SW and SE. This product overestimates precipitation in most ranges, showing the lowest reliability (Figure 12). In the NW basin, CGS01 yields the lowest annual precipitation of 165.1 mm. Error analysis (Figure 9) indicates that CGS01 overestimates precipitation in this range, suggesting that the actual precipitation may be lower than the estimated value, and CGS01 is closest to the real value. Similarly, in the SHR, LR, HaiR, and YeR basins, where annual precipitation is approximately 500 mm, WRB values are close to or slightly lower than those of CGS01, and CHM_PRE_V2 agrees well with CGS01. Slight overestimation still exists in CGS01 in this range, implying that the actual precipitation may be marginally lower than CGS01. Overall, WRB, CGS01, and CHM_PRE_V2 show the highest reliability. In the HuaiR and YZR basins with annual

https://doi.org/10.5194/essd-2026-564
Preprint. Discussion started: 15 October 2026
© Author(s) 2026. CC BY 4.0 License.



precipitation around 1000 mm, the relative bias of CGS01 is close to 0%, indicating the most credible results. In the SE and ZHR basins with annual precipitation near 1500 mm, the relative bias of CGS01 is negative but near 0%. In the SE basin, CMFD_V1 estimates much higher precipitation over Taiwan Province than other products, leading to an obviously higher basin-averaged value and lower reliability; thus, CGS01 is the most reliable. The SW basin, mostly located on the Qinghai-Tibet Plateau, is characterized by sparse gauge networks and complex terrain, where CGS01 performs significantly better than other products (Figure 6). At the national scale, WRB, CMFD_V1, and CN05.1 show similar magnitudes and relatively low reliability. Synthetic analysis demonstrates that CGS01 has the highest reliability in annual precipitation across China and all first-level basins, while CHM_PRE_V2, which is close to CGS01 in most basins, ranks second (Figure 12). From 2000 to 2024, the annual average precipitation across China was 600.9 mm, with a significant increasing trend of 2.6 mm per year.

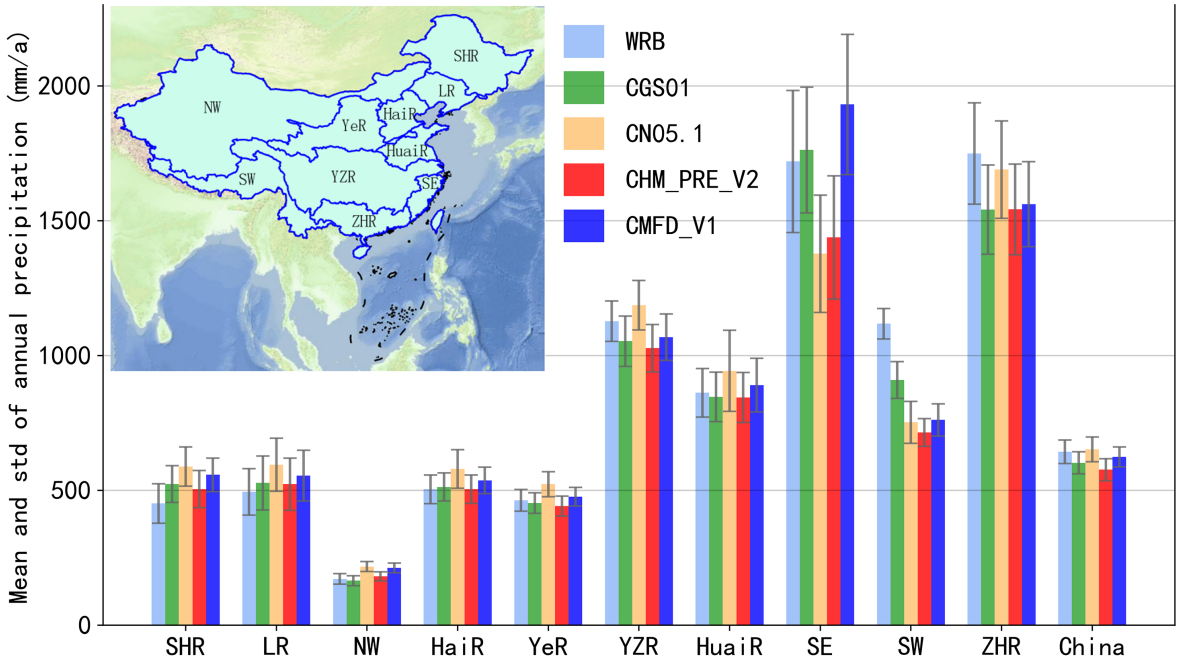


Figure 12. Mean and standard deviation of annual precipitation (2005-2018).

Regarding annual trends of 2005-2018, CN05.1 shows negative trends in all basins and nationwide, which is inconsistent with the consensus that precipitation has increased in most basins under global warming, resulting in the lowest reliability. Except for the SW, SE, and ZHR basins, trends from other products are relatively consistent across basins: only the HuaiR basin shows a negative trend, while all others show positive trends, which conforms to the general understanding of increased precipitation under global warming (Figure 13). From 2000 to 2024, eight out of China's ten first level watersheds showed wetting trends, with trends ranging from 0.5 to 8.4 mm per year.

https://doi.org/10.5194/essd-2026-564
Preprint. Discussion started: 15 October 2026
© Author(s) 2026. CC BY 4.0 License.

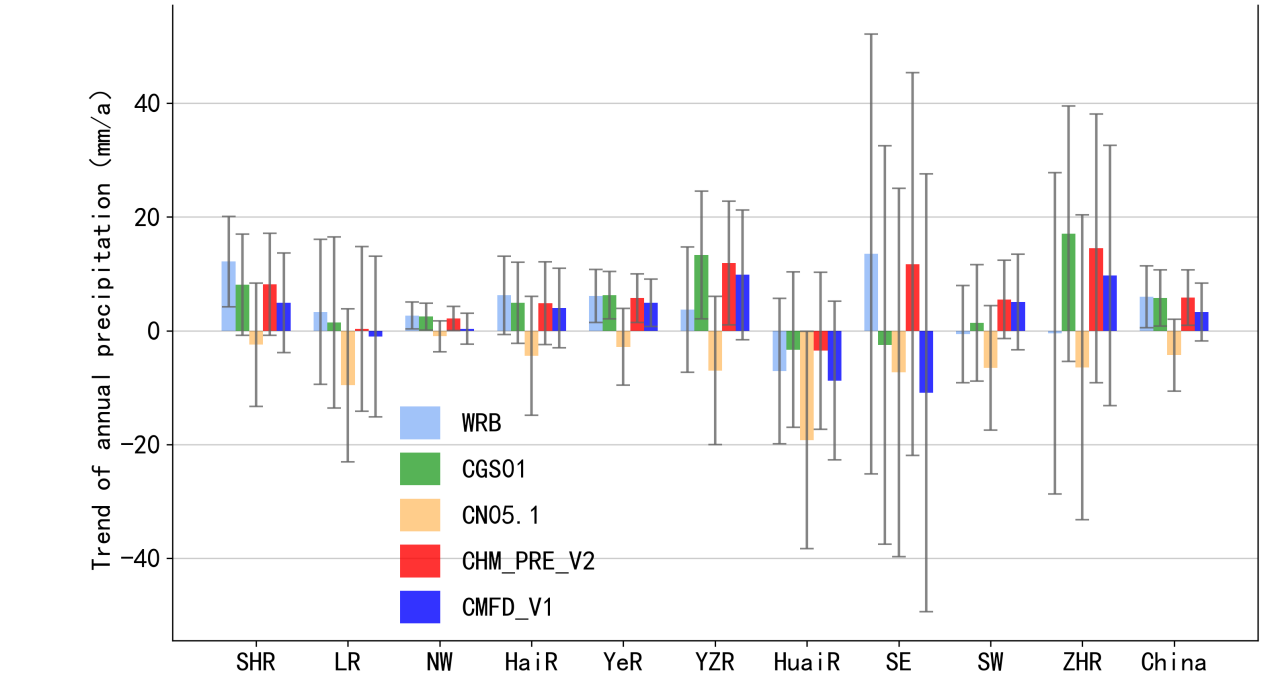


Figure 13. Trend of annual precipitation (2005-2018) based on Theil-Sen estimation at 95% confidence level.

3.5 Changes in Daily Extreme Precipitation in First-Level Watersheds of China

Investigating changes in extreme precipitation can not only reveal the actual evolution of extreme precipitation within each basin and provide data support for global change research, but also examine the reliability of precipitation products to a certain extent by analyzing the consistency between observed changes and global change theories. In hydrological studies, rainstorms are usually defined by explicit uniform thresholds. However, since the study area spans from arid to humid regions, applying a uniform rainstorm threshold cannot objectively reflect the variations in daily extreme precipitation across different basins. Therefore, basin-specific extreme precipitation thresholds are adopted in this study. The threshold is determined by constructing a frequency distribution of daily precipitation from all pixels within each basin during 2000–2024, with the daily precipitation value corresponding to a cumulative frequency exceeding 99% used as the threshold for daily extreme precipitation in that basin.

Daily extreme precipitation shows a significant increasing trend in most first-level river basins across China, which is consistent with the consensus that extreme precipitation events have generally intensified under global warming. Among the ten first-level river basins nationwide, daily extreme precipitation exhibits a significant increasing trend in seven basins, a decreasing trend in one basin, and a relatively stable trend in two basins (Figure 14). The changing rates of the proportion of daily extreme precipitation in total precipitation for the NW, LR, YeR, SHR, HaiR, YZR, and HuaiR basins are 0.2%/a, 0.5%/a, 0.2%/a, 0.4%/a,

https://doi.org/10.5194/essd-2026-564
Preprint. Discussion started: 15 October 2026
© Author(s) 2026. CC BY 4.0 License.



0.4%/a, 0.2%/a, and 0.3%/a, respectively. Total precipitation also shows an increasing trend in all these basins except HuaiR, indicating that daily extreme precipitation is increasing at a faster rate. The corresponding changing rates of daily extreme precipitation amount are 0.4 mm/a, 2.7 mm/a, 1.6 mm/a, 2.4 mm/a, 2.7 mm/a, 2.0 mm/a, and 1.8 mm/a, respectively. Daily extreme precipitation in the SE basin shows a decreasing trend, with the changing rate of its proportion in total precipitation and the changing rate of its amount being -0.2%/a and -2.9 mm/a, respectively. Daily extreme precipitation in the SW and ZHR basins is generally stable. The changing rates of the extreme precipitation proportion are both 0%/a, and the changing rates of the precipitation amount are -0.5 mm/a and 0.5 mm/a, respectively.

4 Discussion

4.1 Methods comparison and analysis

Methods comparison and analysis help to identify the most suitable approach for specific application purposes from a variety of methods, avoiding confusion caused by inconsistent results from multiple concurrent methods. Methods comparison should be carried out based on the fundamental principles of the methods and combined with accuracy evaluation results. There are two main difficulties in regional precipitation estimation: First, the density of gauge stations is insufficient to characterize the high-frequency spatial variations in precipitation, even in eastern China with relatively dense gauges, and this problem is especially severe in alpine and canyon regions of western China. Therefore, how to obtain fine-scale spatial variation information of precipitation is the primary challenge. Second, interpolation methods for spatial extrapolation from point gauges to regional grids differ greatly in their characteristics and advantages. Three main approaches are used to obtain high-frequency spatial variation information of precipitation: First, satellite-based precipitation observations, such as GPM. Second, proxy-based methods, which indirectly estimate precipitation using auxiliary information such as terrain and elevation. CN05.1 using DEM as a covariate in the thin-plate spline method, CHM_PRE_V1 adopting the PRISM model (Daly et al., 2002) for local multiple linear regression, and CHM_PRE_V2 using the LGBM machine learning algorithm all fall into this category. Third, climate model-based methods, which use reanalysis data derived from climate model simulations, as represented by CMFD_V1.

Among the three approaches above, GPM satellite precipitation observations have a sound physical basis. After being corrected by the phase-separated(solid / liquid precipitation) and piecewise linear systematic error correction method proposed in this study, it becomes the optimal choice for characterizing high-frequency spatial variations in precipitation. The main limitation of using DEM as a covariate in the thin plate spline method to capture fine spatial precipitation patterns is that the influence of elevation on precipitation is not globally linear. Due to the complexity of atmospheric circulation and surface interactions, the relationship between elevation and precipitation often deviates from general patterns in many regions. In addition, this method has limited ability to represent fine spatial details. These two drawbacks are particularly evident in one-dimensional thin plate spline interpolation and merging, which can only roughly reflect spatial precipitation variations. Significant biases appear in the low-elevation, high-precipitation area of southeastern Xizang Autonomous Region, and the depiction of spatial variations in other sections of the profile is also relatively coarse (Figure 15). This explains why CN05.1 exhibits lower accuracy than other products.

https://doi.org/10.5194/essd-2026-564
Preprint. Discussion started: 15 October 2026
© Author(s) 2026. CC BY 4.0 License.

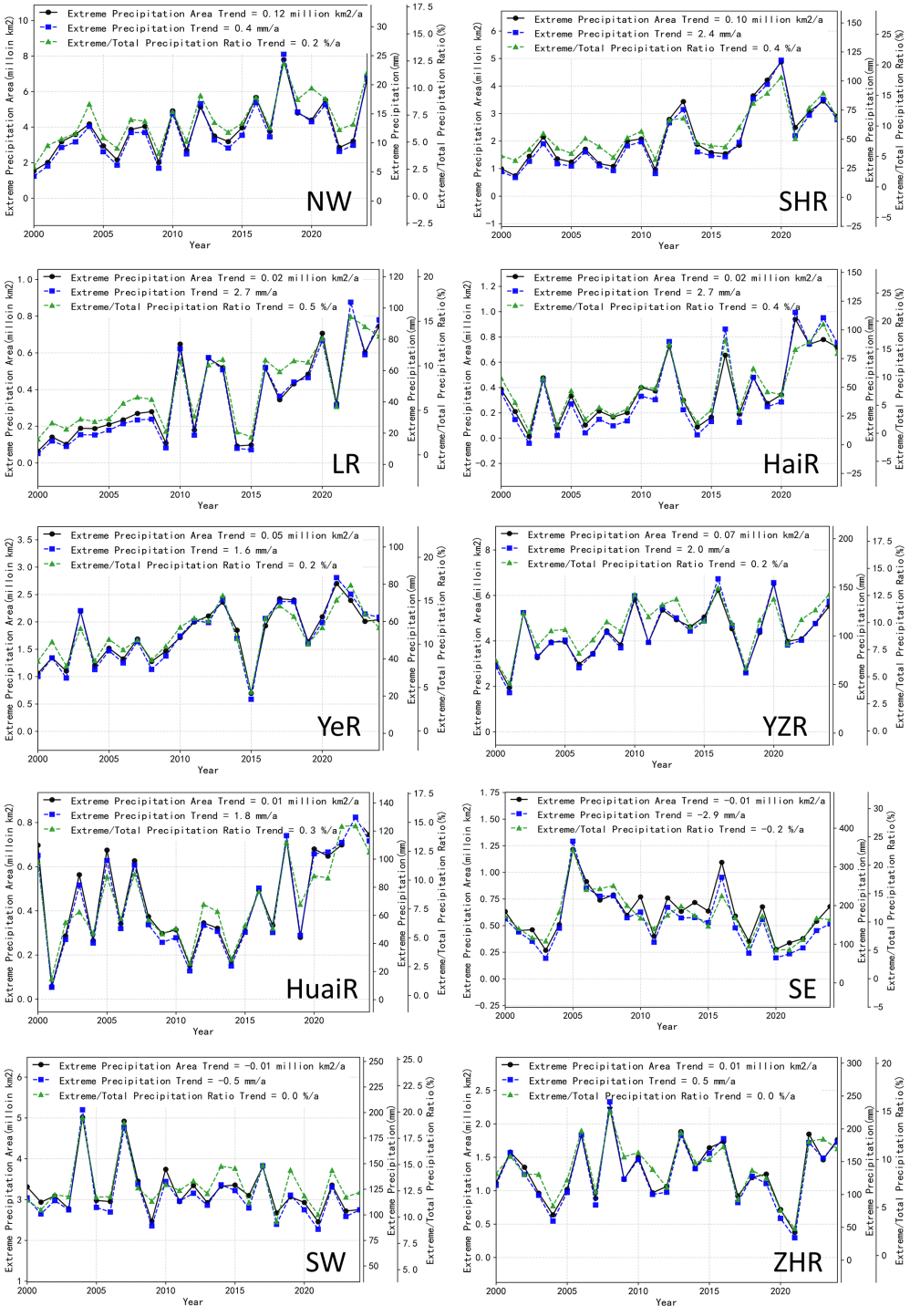


Figure 14. Changes in daily extreme precipitation across first-level watersheds (2000-2024). In seven of the ten first level watersheds, the contribution ratio of daily extreme precipitation to total precipitation increased significantly.

https://doi.org/10.5194/essd-2026-564
Preprint. Discussion started: 15 October 2026
© Author(s) 2026. CC BY 4.0 License.

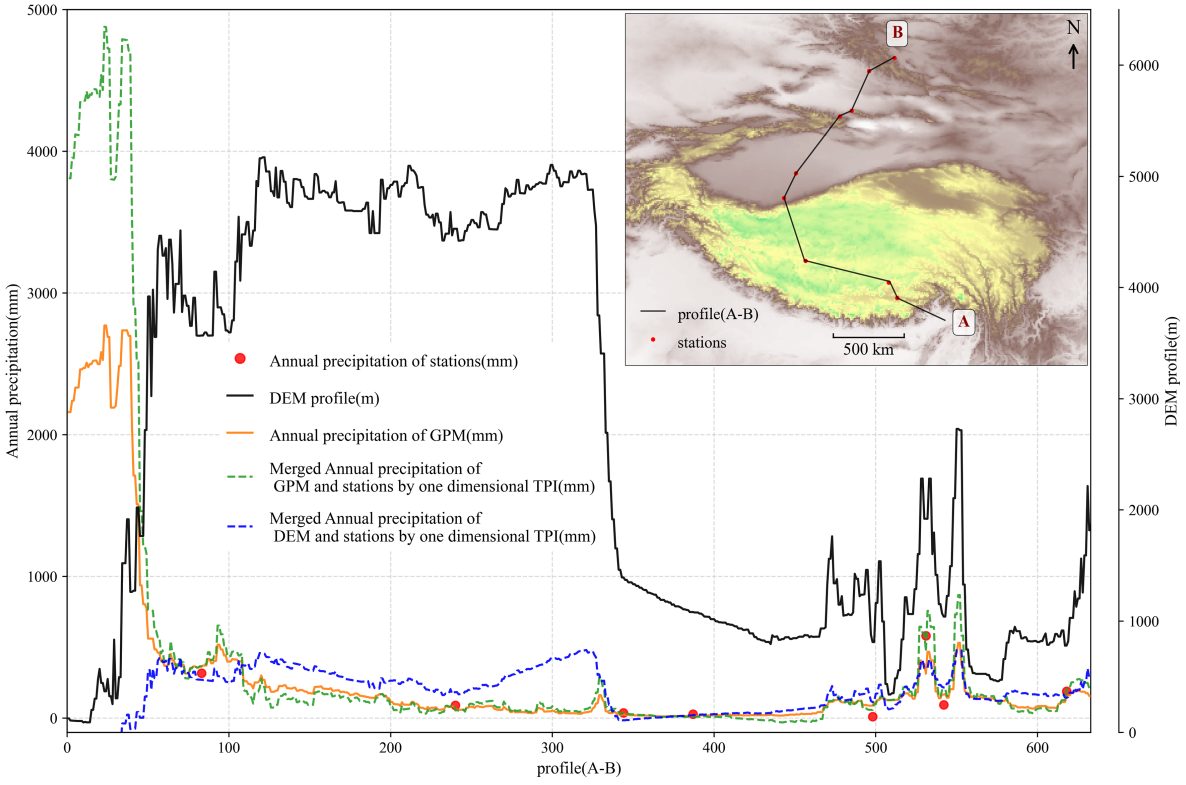


Figure 15. One-Dimensional Thin-Plate Spline Interpolation and Fusion Method. The DEM used as a covariant fails to reproduce the high precipitation values over the southeastern Qinghai–Tibet Plateau.

The PRISM method incorporates additional factors such as wind direction and aspect besides elevation, and adopts local linear regression. It not only considers the diversity of precipitation-controlling factors but also captures regional differences in spatial precipitation patterns. However, since this method develops statistical relationships based on local gauge data, it still relies heavily on station density and is expected to perform poorly in sparsely gauged regions and areas with complex terrain. This should account for why CHM_PRE_V1 is significantly more reliable than CN05.1 (Han et al., 2023).

Nonlinear machine learning algorithms can characterize the spatial distribution of precipitation in finer detail, but they carry extrapolation risks. When extending from “known areas (e.g., low-elevation regions with gauges)” to “unknown areas (e.g., mountain tops without gauges)”, the stability of nonlinear models is often lower than that of linear models. This has been widely recognized as a consensus in hydrology (Daly et al., 2002). The accuracy evaluation in this study also supports this conclusion: at the gauge scale, the annual precipitation accuracy of CHM_PRE_V2 is much higher than other products; at the basin scale with gauge coverage, its water balance accuracy is only slightly higher than CGS01; however, in ungauged alpine and canyon regions of western China, the regularity of precipitation spatial distribution controlled by topography and

https://doi.org/10.5194/essd-2026-564
Preprint. Discussion started: 15 October 2026
© Author(s) 2026. CC BY 4.0 License.



wind direction is significantly weaker than that of CGS01. This is a typical manifestation of over-fitting in nonlinear machine learning.

Although the climate model method has a clear physical foundation and comprehensive consideration of factors, it still cannot finely capture high-frequency spatial precipitation information due to the complex mechanisms governing precipitation spatial patterns. CMFD_V1 yields obviously higher precipitation than other products in the SE basin, with precipitation in ungauged Taiwan Province exceeding 1.5 times that of other products. Moreover, in ungauged alpine and canyon regions of western China, the regularity of precipitation spatial distribution controlled by topography and wind direction is much lower than that of CGS01. All these directly reflect its limitations.

GPM satellite-based precipitation is mainly retrieved from the backscatter intensity of radar signals by hydrometeors, with a sound and reasonable physical basis. Although it suffers from underestimation of heavy precipitation and overestimation of light precipitation (Yu et al., 2022), these issues are common to all precipitation observation methods and not unique to satellite retrievals. Furthermore, the systematic errors caused by such "heavy precipitation underestimation and light precipitation overestimation" can be effectively corrected using the phase-separated (solid / liquid) and piecewise linear method proposed in this study. The high accuracy and strong stability of CGS01 at the gauge scale, gauged basin scale, and ungauged alpine canyon regions strongly validate the effectiveness of this correction approach.

Among interpolation methods, the thin plate spline method is the most widely used global surface interpolation scheme. Its advantages include good performance in fitting smooth surfaces, no need for manually tuned empirical parameters, and high reproducibility. Its disadvantage is that it is not suitable for fitting discontinuous or sharply varying information. The inverse distance weighting (IDW) method is a widely used local surface interpolation method. The optimal interpolation method uses IDW to interpolate the precipitation differences between satellite and gauge observations (Nie et al., 2016). Both CHM_PRE_V1 and CHM_PRE_V2 have improved this method and recommended the modified IDW approach (Hu et al., 2025). IDW is advantageous in fitting discontinuous or highly variable spatial patterns, but it requires empirical parameters such as the power exponent, correlation decay distance, and minimum number of stations. Empirical parameters calibrated for China may not be applicable to other regions.

Annual precipitation fields or daily climatological precipitation fields (generated from multi-year daily mean precipitation or Fourier truncation) are usually spatially smooth. The thin plate spline method is recommended to fully exploit its strength in fitting smooth surfaces and avoid manual parameter tuning. For the interpolation of daily precipitation ratios or anomalies, some comparative studies have reported that IDW outperforms thin plate splines. However, these studies did not analyze the dependence of the two methods on interpolation distance, so they cannot verify the superiority of IDW in sparsely gauged regions (Hu et al., 2025). In addition, this study achieves better performance using the thin plate spline method than CHM_PRE_V2. As an upgraded product of CHM_PRE_V1 from the same research team, CHM_PRE_V2 has significantly higher accuracy than its predecessor. Therefore, the thin-plate spline method is recommended in this study.

https://doi.org/10.5194/essd-2026-564
Preprint. Discussion started: 15 October 2026
© Author(s) 2026. CC BY 4.0 License.


4.2 Performance in water balance analysis

Water budget closure serves as a core criterion for verifying the reliability of hydrological cycle observations and models, accurately identifying hydrological cycle trends under climate change, and supporting water resources management and climate decision-making. Its difficulty stems primarily from large observational errors, uneven spatial-temporal distribution, and discontinuous data for key components such as evaporation, precipitation, groundwater, and glaciers, along with unobservable processes like atmospheric water vapor transport and groundwater recharge, human activity disturbances, and scale mismatches and inconsistencies across different observation platforms and models—all of which collectively make water budget balancing challenging from global to watershed scales. Taking precipitation as an example, regional precipitation errors is large, especially in areas with sparse stations, uneven distribution, and alpine-valley terrain. Using the precipitation product in this study as input to the Budyko water-energy equation, the simulated annual runoff has an error of approximately 10% relative to observed runoff (with observed runoff as the benchmark). This indicates a high consistency between the two independent hydrological cycle variables (precipitation and runoff) from different sources, and their variations conform to hydrological cycle principles. The method proposed in this study is insensitive to the number and density of observation stations, with errors expected to be comparable in station-free and alpine-valley areas to those in areas with stations. These findings strongly demonstrate that the CGS01 product achieves errors close to 10% in water budget analyses across all national watersheds. Generally, observed runoff errors are approximately 6%–19% (Harmel et al., 2006), and the performance of the CGS01 product matches this range, meaning precipitation error is no longer a major obstacle to water budget closure in water balance analyses.

4.3 Error Sources and Characteristics of GPM

There are three main error sources of GPM: first, the large spatial scale mismatch between gauge and satellite observations, which affects the rationality of direct comparison; second, the precipitation phase; third, the deviation of the random error distribution from the normal distribution. The scale mismatch exerts a strong influence at short timescales but a relatively weak influence at long timescales. With temporal accumulation, the random errors caused by scale mismatch can be significantly reduced, which is one reason why the consistency between satellite and gauge observations is much higher at the annual scale than at the daily scale. Snow particles and raindrops exhibit different scattering characteristics for radar waves. The dual-frequency precipitation radar retrieval algorithm onboard the GPM core satellite targets liquid precipitation by default, leading to systematic underestimation of snowfall (Speirs et al., 2017; Bertoncini et al., 2025). The random error distribution of daily precipitation observations deviates from normality, characterized by underestimation of heavy precipitation and overestimation of light precipitation. This explains the S-shaped pattern of annual precipitation systematic error: annual precipitation tends to be underestimated when heavy precipitation accounts for a large proportion, and overestimated when light precipitation dominates.

Some researchers suggest that surface snow cover can enhance radar echoes reflected from the ground, leading to overestimation in satellite-based precipitation retrievals (Mroz et al., 2021). In this study, we analyzed the impact of surface snow cover on GPM precipitation observations by classifying and statistically comparing daily precipitation data for snow-covered

https://doi.org/10.5194/essd-2026-564
Preprint. Discussion started: 15 October 2026
© Author(s) 2026. CC BY 4.0 License.



and snow-free conditions from 2000 to 2024. Surface snow cover was identified using the MODIS MOD10A2 snow product, which has an 8-day temporal resolution. A pixel was classified as snow-covered for the entire 8-day period if it was identified as snow in two consecutive retrievals; otherwise, it was classified as snow-free. Statistical results show that GPM systematically underestimates snowfall regardless of surface snow cover. The average underestimation is 44% under snow-covered surface conditions and 40% under snow-free conditions, with a small difference of only 4 percentage points, indicating that snow cover has no impact on GPM precipitation observations.

4.4 Implications for Global Precipitation Mapping

Theoretical calculations indicate that global precipitation increases by 2.0% for every 1°C rise in global temperature (Zhang et al., 2024). Increased precipitation can accelerate the release of heat from the Earth system and largely offset the suppression of thermal radiation loss caused by rising greenhouse gas concentrations. Due to the lack of high-precision global precipitation datasets, the heat dissipated through precipitation cannot be accurately quantified, and the coupled interactions among precipitation, air temperature, and radiation cannot be thoroughly analyzed. This constitutes the fundamental cause of the low reliability of precipitation projections under global cimatic change.

The method proposed in this study can effectively address the longstanding challenge of quantifying global land precipitation. Although global precipitation gauges suffer from uneven distribution and sparse coverage (Su et al., 2026), the present method is insensitive to station density, maintains high reliability in alpine and canyon regions, and exhibits strong extrapolation capability. It is estimated that high-precision global land precipitation quantification can be achieved using the existing gauge network. The final accuracy depends on the representativeness of gauge observations in terms of global annual precipitation amount and its structure. As long as gauge observations cover a nearly complete and uniform spectrum from light to heavy precipitation, and the precipitation structure is representative of different climate zones, systematic errors can be estimated and corrected for different annual precipitation ranges. For instance, precipitation gauges are extremely sparse over Africa, making direct independent validation of satellite precipitation products difficult (Su et al., 2026). Gauge observations from the same latitudinal zones on other continents can be regarded as representative of the annual precipitation amount and structure over corresponding climate regions in Africa, thereby enabling high-precision precipitation quantification over the African continent.

For oceanic precipitation, however, its annual amount and temporal structure differ significantly from those over land. Direct transfer of systematic error functions derived from land gauges to oceans would introduce considerable uncertainty. Instead, the total annual oceanic precipitation can be estimated from the land-ocean annual precipitation ratio derived from reanalysis datasets. The global land-ocean precipitation ratio is relatively stable at the inter-annual scale, with only small fluctuations modulated by tropical air-sea interaction events such as El Niño. Reanalysis data can well characterize the impacts of such events on land-ocean precipitation partitioning and their spatiotemporal variations. This provides a feasible solution to accurate precipitation estimation over oceans under extreme scarcity of in-situ observations, and supports more reliable research on the role of precipitation in the global energy balance and global precipitation changes under warming.

https://doi.org/10.5194/essd-2026-564
Preprint. Discussion started: 15 October 2026
© Author(s) 2026. CC BY 4.0 License.



5 Data availability

The CGS01 daily precipitation dataset (2000–2024) covers the entire terrestrial areas of China at a spatial resolution of 0.1°. The dataset will be updated annually. All data are provided in GeoTIFF format and can be freely accessed at https://doi.org/10.5281/zenodo.20176004 (Yan et al., 2026).

6 Conclusions

Precipitation exhibits strong spatial heterogeneity. Reliance solely on gauge observations hardly enables the high-precision quantification of regional precipitation spatial distribution, necessitating the integration of high-frequency spatial variation information of regional precipitation with in-situ gauge data. Compared with alternative estimation methods (e.g., terrain-based interpolation) and reanalysis datasets, satellite observations present distinct advantages in reliability; nevertheless, systematic error correction and random error reduction are indispensable.

The dual thin-plate spline fusion method proposed in this study fully leverages the superior spatial coverage of satellite observations and the high local accuracy of gauge measurements, effectively addressing precipitation estimation challenges in gauge-sparse regions and areas with intense topographic undulation. In China, the CGS01 precipitation dataset was generated by merging GPM data with sparse gauge records (accounting for only 27% of the gauge density used in previous studies). Nationally, the average relative error of annual precipitation for CGS01 is 2%, and the error in watershed water balance analysis is 10.9% (referencing observed runoff as the benchmark). This dataset can reasonably reproduce the controls of topography and wind direction on precipitation spatial patterns in alpine and canyon regions without ground gauges. The correlation coefficient, KGE, POD, and MAE of CGS01 are 0.80, 0.72, 0.91, and 1.69 mm/d, respectively. Compared with CHM_PRE_V2, CGS01 improves the above metrics by 14.2%, 2.9%, 21.3%, and 8.2%.

From 2000 to 2024, the national mean annual precipitation of China was 600.9 mm, with an annual increasing rate of 2.6 mm and eight out of China's ten first level watersheds showed annually wetting trends, with trends ranging from 0.5 to 8.4 mm per year. Nationwide, daily extreme precipitation has increased rapidly. In seven of the ten first level watersheds, the contribution ratio of daily extreme precipitation to total precipitation increased at a rate of 0.2%-0.5% per year.

Author contributions. Bokun Yan and Wenpeng Li contributed to designing the research; Bokun Yan implemented the research and wrote original draft; Wenpeng Li supervised the research; all co-authors revised the manuscript and contributed to the writing.

Competing interests. The contact author has declared that none of the authors has any competing interests.

https://doi.org/10.5194/essd-2026-564
Preprint. Discussion started: 15 October 2026
© Author(s) 2026. CC BY 4.0 License.



Acknowledgements. The work was supported by Heihe Field Station Open Foundation Project and Water Resource Survey Project of China Geological Survey (Grant WCSHR-2025-05, [2026]05-1-015-02 and [2023]04-01-03). We also thank CMA, MWRC, NOAA, and NASA for their data sharing.

https://doi.org/10.5194/essd-2026-564
Preprint. Discussion started: 15 October 2026
© Author(s) 2026. CC BY 4.0 License.



References

Baez-Villanueva, O.M., Zambrano-Bigiarini, M., Beck, H.E., McNamara, I., Ribbe, L., Nauditt, A., Birkel, C., Verbist, K., Giraldo-Osorio, J.D., Xuan Thinh, N., 2020. RF-MEP: A novel Random Forest method for merging gridded precipitation products and ground-based measurements. Remote Sensing of Environment 239, 111606. https://doi.org/10.1016/j.rse.2019.111606

Bertoncini, A., Thériault, J.M., Pomeroy, J.W., 2025. A New GPM-DPR Algorithm to Estimate Snowfall in Mountain Regions. JGR Atmospheres 130, e2024JD041481. https://doi.org/10.1029/2024JD041481

Christian, J.I., Basara, J.B., Hunt, E.D., Otkin, J.A., Furtado, J.C., Mishra, V., Xiao, X., Randall, R.M., 2021. Global distribution, trends, and drivers of flash drought occurrence. Nat Commun 12, 6330. https://doi.org/10.1038/s41467-021-26692-z

Cohen, S., Pincus, R., 2025. A spectroscopic theory for how mean rainfall changes with surface temperature. Science Advances. https://doi.org/10.1126/sciadv.adv6191

Daly, C., Gibson, W., Taylor, G., Johnson, G., Pasteris, P., 2002. A knowledge-based approach to the statistical mapping of climate. Clim. Res. 22, 99–113. https://doi.org/10.3354/cr022099

Dorigo, W., Dietrich, S., Aires, F., Brocca, L., Carter, S., Cretaux, J.-F., Dunkerley, D., Enomoto, H., Forsberg, R., Güntner, A., Hegglin, M.I., Hollmann, R., Hurst, D.F., Johannessen, J.A., Kummerow, C., Lee, T., Luojus, K., Looser, U., Miralles, D.G., Pellet, V., Recknagel, T., Vargas, C.R., Schneider, U., Schoeneich, P., Schröder, M., Tapper, N., Vuglinsky, V., Wagner, W., Yu, L., Zappa, L., Zemp, M., Aich, V., 2021. Closing the Water Cycle from Observations across Scales: Where Do We Stand? Bulletin of the American Meteorological Society 102, E1897–E1935. https://doi.org/10.1175/BAMS-D-19-0316.1

Fang, J., Yang, W., Luan, Y., Du, J., Lin, A., Zhao, L., 2019. Evaluation of the TRMM 3B42 and GPM IMERG products for extreme precipitation analysis over China. Atmospheric Research 223, 24–38. https://doi.org/10.1016/j.atmosres.2019.03.001

Gebrechorkos, S.H., Sheffield, J., Vicente-Serrano, S.M., Funk, C., Miralles, D.G., Peng, J., Dyer, E., Talib, J., Beck, H.E., Singer, M.B., Dadson, S.J., 2025. Warming accelerates global drought severity. Nature 642, 628–635. https://doi.org/10.1038/s41586-025-09047-2

Han, J., Miao, C., Gou, J., Zheng, H., Zhang, Q., Guo, X., 2023. A new daily gridded precipitation dataset for the Chinese mainland based on gauge observations. Earth Syst. Sci. Data 15, 3147–3161. https://doi.org/10.5194/essd-15-3147-2023

Harmel, R.D., Cooper, R.J., Slade, R.M., Haney, R.L., Arnold, J.G., 2006. Cumulative uncertainty in measured streamflow and water quality data for small watersheds. Transactions of the ASABE 49, 689–701. https://doi.org/10.13031/2013.20488

Hayder, K.H., Nassrullah, S.A., 2025. Impact of climate changes on Arizona State precipitation patterns using high-resolution climatic gridded datasets. Journal of Groundwater Science and Engineering, 13(1): 34–46. https://doi.org/10.26599/JGSE.2025.9280037

He, J., Yang, K., Tang, W., Lu, H., Qin, J., Chen, Y., Li, X., 2020. The first high-resolution meteorological forcing dataset for land process studies over China. Sci Data 7, 25. https://doi.org/10.1038/s41597-020-0369-y

Hu, J., Miao, C., Su, J., Zhang, Q., Gou, J., Sun, Q., 2025. A new upgraded high-precision gridded precipitation dataset considering spatiotemporal and physical correlations for mainland China. https://doi.org/10.5194/essd-2025-20

Huffman, G.J., Bolvin, D.T., Nelkin, E.J., Wolff, D.B., Adler, R.F., Gu, G., Hong, Y., Bowman, K.P., Stocker, E.F., 2007. The TRMM Multisatellite Precipitation Analysis (TMPA): Quasi-Global, Multiyear, Combined-Sensor Precipitation Estimates at Fine Scales. Journal of Hydrometeorology 8, 38–55. https://doi.org/10.1175/JHM560.1

Hutchinson, M.F., 1995. Interpolating mean rainfall using thin plate smoothing splines. International journal of geographical information systems 9, 385–403. https://doi.org/10.1080/02693799508902045

© Author(s) 2026. CC BY 4.0 License.



Hutchinson, M.F., McKenney, D.W., Lawrence, K., Pedlar, J.H., Hopkinson, R.F., Milewska, E., Papadopol, P., 2009. Development and Testing of Canada-Wide Interpolated Spatial Models of Daily Minimum–Maximum Temperature and Precipitation for 1961–2003. Journal of Applied Meteorology and Climatology 48, 725–741. https://doi.org/10.1175/2008JAMC1979.1

Jin, C., Wang, B., Cheng, T.F., Dai, L., Wang, T., 2024. How much we know about precipitation climatology over Tianshan Mountains—the Central Asian water tower. npj Clim Atmos Sci 7, 21. https://doi.org/10.1038/s41612-024-00572-x

Jiang, Y., Tang, W., Yang, K., He, J., Shao, C., Zhou, X., Lu, H., Chen, Y., Li, X., Shi, J., 2025. Development of a high-resolution near-surface meteorological forcing dataset for the Third Pole region. Sci. China Earth Sci. 68, 1274–1290. https://doi.org/10.1007/s11430-024-1507-6

Jiang, Y., Yang, K., Yang, H., Lu, H., Chen, Y., Zhou, X., Sun, J., Yang, Y., Wang, Y., 2022. Characterizing basin-scale precipitation gradients in the Third Pole region using a high-resolution atmospheric simulation-based dataset. Hydrol. Earth Syst. Sci. 26, 4587–4601. https://doi.org/10.5194/hess-26-4587-2022

Joyce, R.J., Janowiak, J.E., Arkin, P.A., Xie, P., 2004. CMORPH: A Method that Produces Global Precipitation Estimates from Passive Microwave and Infrared Data at High Spatial and Temporal Resolution. J. Hydrometeor 5, 487–503. https://doi.org/10.1175/1525-7541(2004)005<0487:CAMTPG>2.0.CO;2

Kuang, X., Liu, J., Scanlon, B.R., Jiao, J.J., Jasechko, S., Lancia, M., Biskaborn, B.K., Wada, Y., Li, H., Zeng, Z., Guo, Z., Yao, Y., Gleeson, T., Nicot, J.-P., Luo, X., Zou, Y., Zheng, C., 2024. The changing nature of groundwater in the global water cycle. Science 383, eadf0630. https://doi.org/10.1126/science.adf0630

Liu, J., Du, J., Yang, Y., Wang, Y., 2020. Evaluating extreme precipitation estimations based on the GPM IMERG products over the Yangtze River Basin, China. Geomatics, Natural Hazards and Risk 11, 601–618. https://doi.org/10.1080/19475705.2020.1734103

Liu, Y., Zheng, Y., Li, W., Zhou, T., 2022. Evaluating the Performance of Satellite-Based Precipitation Products Using Gauge Measurement and Hydrological Modeling: A Case Study in a Dry Basin of Northwest China. Journal of Hydrometeorology 23, 541–559. https://doi.org/10.1175/JHM-D-21-0152.1

Ma, S., Zhou, S., Yu, B., Song, J., 2024. Deforestation-induced runoff changes dominated by forest-climate feedbacks. Sci. Adv. 10, eadp3964. https://doi.org/10.1126/sciadv.adp3964

Maina, F.Z., Kumar, S.V., 2025. Global patterns of rain-on-snow and its impacts on runoff from past to future projections. Nat Commun 16, 4731. https://doi.org/10.1038/s41467-025-59855-3

Mega, T., Ushio, T., Takahiro, M., Kubota, T., Kachi, M., Oki, R., 2019. Gauge-Adjusted Global Satellite Mapping of Precipitation. IEEE Trans. Geosci. Remote Sensing 57, 1928–1935. https://doi.org/10.1109/TGRS.2018.2870199

Miguez-Macho, G., Fan, Y., 2025. A global humidity index with lateral hydrologic flows. Nature 644, 413–419. https://doi.org/10.1038/s41586-025-09359-3

Mroz, K., Montopoli, M., Battaglia, A., Panegrossi, G., Kirstetter, P., Baldini, L., 2021. Cross-validation of active and passive microwave snowfall products over the continental United States. Journal of Hydrometeorology. https://doi.org/10.1175/JHM-D-20-0222.1

Najibi, N., Devineni, N., 2018. Recent trends in the frequency and duration of global floods. Earth Syst. Dynam. 9, 757–783. https://doi.org/10.5194/esd-9-757-2018

Nie, S., Wu, T., Luo, Y., Deng, X., Shi, X., Wang, Z., Liu, X., Huang, J., 2016. A strategy for merging objective estimates of global daily precipitation from gauge observations, satellite estimates, and numerical predictions. Adv. Atmos. Sci. 33, 889–904. https://doi.org/10.1007/s00376-016-5223-y

Pan, X., Wu, H., Chen, S., Nanding, N., Huang, Z., Chen, W., Li, C., Li, X., 2023. Evaluation and Applicability Analysis of GPM Satellite Precipitation over Mainland China. Remote Sensing 15, 2866. https://doi.org/10.3390/rs15112866

https://doi.org/10.5194/essd-2026-564
Preprint. Discussion started: 15 October 2026
© Author(s) 2026. CC BY 4.0 License.



Shen, Z., Yong, B., Yi, L., Wu, H., Xu, H., 2022. From TRMM to GPM, how do improvements of post/near-real-time satellite precipitation estimates manifest? Atmospheric Research 268, 106029. https://doi.org/10.1016/j.atmosres.2022.106029

Speirs, P., Gabella, M., Berne, A., 2017. A Comparison between the GPM Dual-Frequency Precipitation Radar and Ground-Based Radar Precipitation Rate Estimates in the Swiss Alps and Plateau. Journal of Hydrometeorology 18, 1247–1269. https://doi.org/10.1175/JHM-D-16-0085.1

Su, J., Miao, C., Zwiers, F., Beck, H., Jones, P., Sun, Q., Slater, L.J., Berghuijs, W.R., Wada, Y., Rosenfeld, D., Gou, J., Wu, Y., Tarolli, P., Borrelli, P., Panagos, P., Alexander, L.V., Zhang, Q., Hu, J., Min, S.-K., Samaniego, L., Duan, Q., Destouni, G., Marengo, J.A., Modarres, R., Sorooshian, S., 2026. Precipitation observing network gaps limit climate change impact assessment. Nature 652, 119–125. https://doi.org/10.1038/s41586-026-10300-5

Tang, T., Chen, T., Gui, G., 2022. A Comparative Evaluation of Gauge-Satellite-Based Merging Products Over Multiregional Complex Terrain Basin. IEEE J. Sel. Top. Appl. Earth Observations Remote Sensing 15, 5275–5287. https://doi.org/10.1109/JSTARS.2022.3187983

Wang, Q., Zhai, P.-M., Qin, D.-H., 2020. New perspectives on 'warming–wetting' trend in Xinjiang, China. Advances in Climate Change Research 11, 252–260. https://doi.org/10.1016/j.accre.2020.09.004

Wang, M., 2025. Reflections on the water cycle and ecological protection and restoration. Journal of Groundwater Science and Engineering, 13(1): 1–4. https://doi.org/10.26599/JGSE.2025.9280034

Wang, Z., Wang, L.-J., Shen, J.-M., et al., 2024. Groundwater recharge via precipitation in the Badain Jaran Desert, China. Journal of Groundwater Science and Engineering, 12(1): 109–118. https://doi.org/10.26599/JGSE.2024.9280009

Wei, L., Jiang, S., Dong, J., Ren, L., Liu, Y., Zhang, L., Wang, M., Duan, Z., 2023. Fusion of gauge-based, reanalysis, and satellite precipitation products using Bayesian model averaging approach: Determination of the influence of different input sources. Journal of Hydrology 618, 129234. https://doi.org/10.1016/j.jhydrol.2023.129234

Woldemeskel, F.M., Sivakumar, B., Sharma, A., 2013. Merging gauge and satellite rainfall with specification of associated uncertainty across Australia. Journal of Hydrology 499, 167–176. https://doi.org/10.1016/j.jhydrol.2013.06.039

Wu, J., Gao, X., 2013. A gridded daily observation dataset over China region and comparison with the other datasets. Chinese Journal of Geophysics(in Chinese) 56, 1102–1111.

Yan, B., Li, W., Gan, F., Zheng, Y., Bai, J., Wang, L., Li, J., Guo, Y., Li, C., Xing, N., Zhuo, Y., Li, R., 2026. CGS01 - A High Accuracy Daily Precipitation Gridded Dataset (2000–2024) across China (Version V01) [data set]. Zenodo. https://doi.org/10.5281/zenodo.20176004.

Yang, K., Chen, Y., Lazhu, Zhan, C., Ling, X., Zhou, X., Jiang, Y., Yao, X., Lu, H., Ma, X., Ouyang, L., Pan, W., Ren, Y., Shao, C., Tian, J., Wang, Y., Yang, H., Yue, S., Zhang, K., Zhao, D., Zhao, L., Zhou, J., Zou, M., 2023. Cross-sectional rainfall observation on the central-western Tibetan Plateau in the warm season: System design and preliminary results. Sci. China Earth Sci. 66, 1015–1030. https://doi.org/10.1007/s11430-022-1081-4

Yang, Z., Hsu, K., Sorooshian, S., Xu, X., Braithwaite, D., Zhang, Y., Verbist, K.M.J., 2017. Merging high-resolution satellite-based precipitation fields and point-scale rain gauge measurements—A case study in Chile. JGR Atmospheres 122, 5267–5284. https://doi.org/10.1002/2016JD026177

Yu, J., Li, X.-F., Lewis, E., Blenkinsop, S., Fowler, H.J., 2020. UKGrsHP: a UK high-resolution gauge–radar–satellite merged hourly precipitation analysis dataset. Clim Dyn 54, 2919–2940. https://doi.org/10.1007/s00382-020-05144-2

Yu, L., Leng, G., Python, A., 2022. A comprehensive validation for GPM IMERG precipitation products to detect extremes and drought over mainland China. Weather and Climate Extremes 36, 100458. https://doi.org/10.1016/j.wace.2022.100458

https://doi.org/10.5194/essd-2026-564
Preprint. Discussion started: 15 October 2026
© Author(s) 2026. CC BY 4.0 License.



610 Zhang, J., Liu, B., Ren, S., Han, W., Ding, Y., Peng, S., 2024. A 4 km daily gridded meteorological dataset for China from 2000 to 2020. Sci Data 11, 1230. https://doi.org/10.1038/s41597-024-04029-x

Zhang, L., Li, X., Zheng, D., Zhang, K., Ma, Q., Zhao, Y., Ge, Y., 2021. Merging multiple satellite-based precipitation products and gauge observations using a novel double machine learning approach. Journal of Hydrology 594, 125969. https://doi.org/10.1016/j.jhydrol.2021.125969

615 Zhang, W., Zhou, T., Wu, P., 2024. Anthropogenic amplification of precipitation variability over the past century. Science 385, 427–432. https://doi.org/10.1126/science.adp0212

Zhang, Y., Gentine, P., Luo, X.Z., Lian, X., Liu, Y.L., Zhou, S., Michalak, A.M., Sun, W., Fisher, J.B., Piao, S.L., Keenan, T.F., 2022. Increasing sensitivity of dryland vegetation greenness to precipitation due to rising atmospheric CO_2. Nature Communications 13, 4875. https://doi.org/10.1038/s41467-022-32631-3

620 Zhang, Y., Li, C., Chiew, F.H.S., Post, D.A., Zhang, X., Ma, N., Tian, J., Kong, D., Leung, L.R., Yu, Q., Shi, J., Liu, C., 2023. Southern Hemisphere dominates recent decline in global water availability. Science 382, 579–584. https://doi.org/10.1126/science.adh0716

Zhang, Y., Wang, K., 2023. Mapping the representativeness of precipitation measurements in Mainland China. Environ. Res. Lett. 18, 024019. https://doi.org/10.1088/1748-9326/acb2e0